MATERIAL MODEL DEVELOPMENT AND VALIDATION OF A HIGH ENERGY ABSORBING FOAM WHICH USED IN FLYER'S HELMET

PİLOT KASKINDA KULLANILAN YÜKSEK ENERJİ EMİCİ KÖPÜĞÜN MALZEME MODELİNİN OLUŞTURULMASI VE DOĞRULANMASI

EMİN ALP UYANIK

PROF. DR. BORA YILDIRIM

Supervisor

Submitted to

Graduate School of Science and Engineering of Hacettepe University

As a Partial Fulfillment to the Requirements for the Award of the Degree of Master of Science in Mechanical Engineering.

2024

In Memory of My Lovely Father

ABSTRACT

MATERIAL MODEL DEVELOPMENT AND VALIDATION OF A HIGH ENERGY ABSORBING FOAM WHICH USED IN FLYER'S HELMET

Emin Alp UYANIK

Master of Science Degree, Department of Mechanical Engineering
Supervisor: Prof. Dr. Bora YILDIRIM
January 2024, 58 pages

Pilot helmets are exposed to many environmental factors during their use. These environmental factors need to be handled very carefully in order not to adversely affect the user's health. In this sense, one of the biggest concerns of engineers is the impact scenarios that can damage the pilot's brain and even cause death. For this reason, pilot helmet designs need to ensure that the helmet has energy absorbing properties to protect the wearer from impacts and at the same time, the helmet should be lightweight to avoid damage on pilot's neck.

In this thesis, the finite element model of the energy absorbing foam to be used in the pilot helmet has been created and validated. Expanded polystyrene material is used as energy absorbing foam. In order to understand the dynamic properties of the material, uniaxial compression tests were performed at different speeds.
According to the test data obtained, it was modeled in two different ways as crushable foam and low-density foam in LS-Dyna program. A total of four different finite element models were constructed using two different mesh structures for each model.

In order to prove the accuracy of the finite element model and to determine other parameters, impact tests were performed on four different thickness specimens. Comparative results of all models with impact test are presented. As a result, it is found that the results obtained by finite element analysis are close enough to the experimental results.

Keywords: Finite Element Model, Expanded Polystyrene, Impact Testing

ÖZET

PİLOT KASKINDA KULLANILAN YÜKSEK ENERJİ EMİCİ KÖPÜĞÜN MALZEME MODELİNİN OLUŞTURULMASI VE DOĞRULANMASI

Emin Alp UYANIK

Yüksek Lisans, Makina Mühendisliği Bölümü
Tez Danışmanı: Prof. Dr. Bora YILDIRIM
Ocak 2024, 58 sayfa

Pilot kaskları kullanımları sırasında birçok çevresel etmene maruz kalırlar. Kullanıcının sağlığını kötü yönde etkilememesi için bu çevresel etmenlerin çok dikkatli bir şekilde ele alınması gerekmektedir. Bu anlamda mühendislerin en büyük endişelerinden birisi pilotun beyninde hasar bırakabilecek hatta ölümüne sebep olabilecek çarpma senaryolarıdır. Bu sebeple pilot kaskı tasarımlarında, kaskın kullanıcıyı çarpmalardan koruyacak yapıda olmasına ve aynı zamanda pilotun boynuna yük bindirmemek için kaskın hafif olmasına dikkat edilmelidir.

Bu tezde, pilot kaskında kullanılacak olan enerji sönümleyici köpüğün sonlu elemanlar modelini oluşturulma ve bu modeli doğrulama çalışmaları gerçekleştirilmiştir. Enerji sönümleyici köpük olarak genleştirilmiş polistren malzemesi kullanılmıştır. Malzemenin dinamik özelliklerini anlamak için öncelikle farklı hızlarda tek eksenli basma testleri yapılmıştır.

Elde edilen test verilerine göre LS-Dyna programında ezilebilir köpük ve düşük yoğunluklu köpük olarak iki farklı şekilde köpük modellemesi yapılmıştır. Her bir model için iki farklı ağ yapısı kullanılarak toplamda dört farklı sonlu elemanlar modeli kurulmuştur.

Hazırlanan sonlu elemanlar modelinin doğruluğunu kanıtlamak ve diğer parametrelerin tespiti için dört farklı kalınlıktaki numuneye darbe testi yapılmıştır. Tüm modellerin darbe deneyi ile karşılaştırmalı sonuçları sunulmuştur. Sonuç olarak, sonlu elemanlar analizi ile elde edilen sonuçların deneysel sonuçlara yeterince yakın olduğu tespit edilmiştir.

Anahtar Kelimeler: Sonlu Elemanlar Modeli, Genleştirilmiş Polistren, Çarpışma Testi

ACKNOWLEDGEMENTS

I would like to express my gratitude to my thesis supervisor Prof. Dr. Bora Yıldırım for his guidance, support, contributions and trust in me throughout this thesis.

I also would like to express my deepest gratitude to my mentor Dr. Taner Kalaycıoğlu and for his leading guidance, helpful critics and technical supports at every step of this study. I would also like to thank him for helping and supporting me to improve my technical background since I started working with him.

I would like express my sincere gratitude to my leader, Dr. Güvenç Canbaloğlu for making it easier for his technical support and recommendations from beginning to end of this study.

I want to thank my colleagues Öner Murat Akbaba and Onur Okcu for their helpful advice and support.

I want to thank my managers and ASELSAN Inc. for giving me the opportunity to use the testing laboratories during my thesis.

I would like to express my eternal appreciation towards my dear family especially my mother Dilek Uyanık, who helped me to come to these days and always put trust in me.

I am especially thankful to my beloved girlfriend Gökçe Acun, for her love, support, patience and encouragement to complete this study.

TABLE OF CONTENTS

LIST OF FIGURES

LIST OF TABLES

LIST OF SYMBOLS & ABBREVIATIONS

List of Symbols

ρ^*	Density of Foam
ρ_s	Density of Solid (Matrix) Material
V_s	Volume of Solid
V_T	Total Volume
I	Moment of Inertia
σ	Stress
ε	Strain
F	Force
δ	Displacement
E_S	Young's Modulus of Solid
E^*	Young's Modulus of Foam
G^*	Shear Modulus of Foam
E	Young's Modulus
G	Shear Modulus
ν	Poisson's Ratio
ν^*	Poisson's Ratio of Foam
P_{cr}	Critical Buckling
l	Length
t	Thickness
n	Number of Buckling Mode Shape
σ_{el}	Elastic Buckling Stress
σ_{el}^*	Elastic Buckling Strength of Foam
M_p	Plastic Moment
σ_{ys}	Yield Stress
M	Moment
σ_{pl}^*	Plastic Strength of Foam
M_f	Fracture Moment
σ_{fs}	Fracture Stress of Solid

σ_{cr}	Crushing Stress
ε_D	Densification Strain
δ_e	Displacement of Bending Edges
F_e	Applied Force to Bending Edges
σ_f	Stress on Stretching Face
ε_f	Strain of Stretching Face
v_f	Volume of Stretching Face
φ	Volume Fraction of Solid in Cell Edges
t_e	Thickness of Edge
t_f	Thickness of Face
V_0	Undeformed Volume
V_g	Volume of Gas
V_g^0	Initial Volume of Gas
p	Gas Pressure
p_0	Initial Gas Pressure
E_g^*	Young's Modulus Contribution of Gas
$\sigma^*_{post-collapse}$	Post Collapse Strength of Foam
σ^*_{pl}	Plastic Collapse Strength of Foam
σ^*_{cr}	Crushing Strength of Foam
a	Acceleration
c	Speed of Sound
Δt	Time Step
$n(\varepsilon)$	Strain Rate sensitivity
a, b	Empirical Constants of Strain Rate Sensitivity
$C_1, C_2, C_3, C_4, C_5, C_6$	Empirical Material Constants of Foams

List of Abbreviations

CAD	Computer Aided Design
CFL	Courant Friedrich Levy
EPS	Expanded Polystyrene
FEA	Finite Element Analysis
MAT_057	Low-Density-Foam Material Card of LS-Dyna
MAT_063	Crushable Foam Material Card of LS-Dyna
WSTC	Wayne State Tolerance Curve

1. INTRODUCTION

1.1. Introduction to Crushable Foams

Foams are used universally in a wide range of applications due to their low cost, high energy absorption capabilities, lightweight and ease of application. Owing to their application areas, a vast range of foams with significantly varied characteristics adapted individually to each end use has been developed. In fact, one of the primary elements contributing to the difficulty of foam modeling is variability.

Two important parameters affecting the characteristics of foam are the matrix material and the structure of gas containing cells. The stiffness behavior of matrix material can be rigid or flexible. Crushable foams consist rigid matrix material which has little or no deformation recovery. Metallic foams and rigid polyurethane foams can be given as examples of crushable foams. While metallic foams undergo deformation by ductile plasticity with little recovery, rigid polyurethane foams undergo deformation by brittle failure and there is no recovery. [1]

Open and closed cells are two generic morphologies used in foams. Open cells connected through open faces to allow free flow fluctuations while closed cells capture blowing gas in a closed volume. Volume fractions of open and closed cells and their pore size have a crucial role on compression behavior of foam.

1.2. Foam Behavior

Foams' excellent and unique energy absorption capabilities under compression is the main reason of common usage in a wide range of application areas. Compression is the most typical mode of deformation in foams since they present high strength only in compression. However, tension or shear modes can occur in foamed components due to their geometry.

Typical foam material has 3 sections in compressive stress-strain curve as seen in Figure 1.1. First region represents elastic deformation and yields to non-elastic plateau compaction region which followed by densification zone.

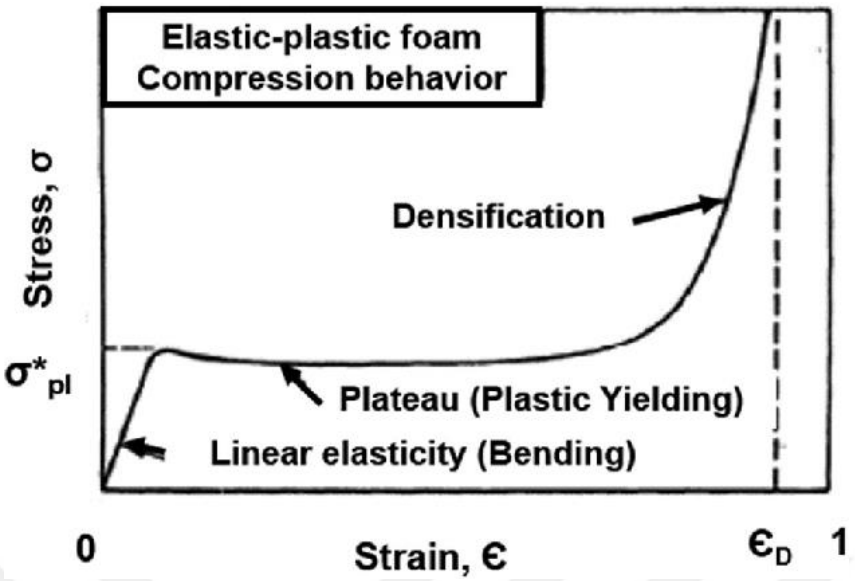

Figure 1.1 Three definite regions typically monitored on foams [2]

In the first region, linear behavior is observed with a slope equal to Young's Modulus. Until the yielding, matrix material dominates the characteristics of the foam due to stiffness of cell wall against to bending for open cells and face stretching for closed cells.

After the yielding, gas component in the cells is strained. The gas flows out from the open cell foams via open pores or channels. On the other hand, the gas is compressed in closed cell foams until collapsing of the cell wall. The collapse of cells is caused by elastic buckling, plastic deformation or brittle crushing depending on matrix material properties.

When all cell elements have ruptured or collapsed, foam behave like matrix material in the densification region and stress increases sharply.

Although the behavior of compressive stress strain curve is same as stated for all foams, size of regions can vary due to the matrix material and the structure of gas containing cells.

1.3. Main Application Areas of Crushable Foams

Crushable foams are used widely with their several advantages which are their enormous energy absorption capability, lightweight, low cost, and ease of application.

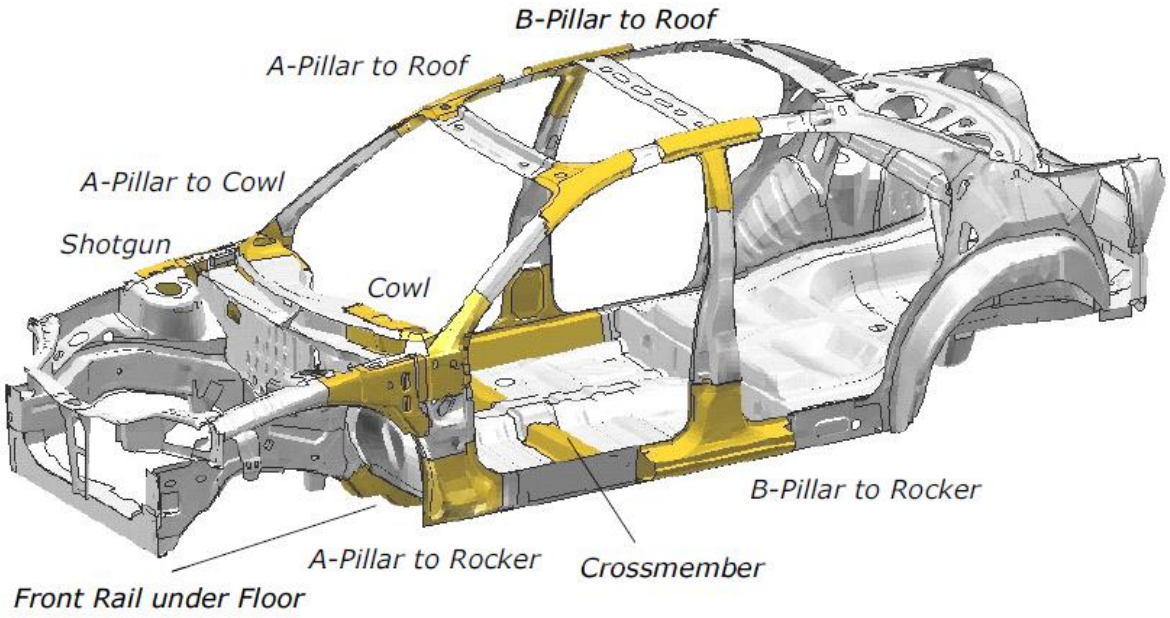

Figure 1.2 Application areas of structural foam for body reinforcement [3]

The first example of application areas for crushable foams can be given as body reinforcement applications. Local reinforcement is a common practice to get stiff car body and good crash performance at the same time. Crushable foams have huge advantages over other reinforcement materials due to their energy absorption capability and lightweight by considering fuel consumption and maneuverability of the car. To illustrate main body reinforcement application areas in car structure are pointed in Figure 1.2.

Figure 1.3 SAFER Barrier [4]

As a second example, crushable foams are used again as energy absorption material for automotive safety. In the design of Steel and Foam Energy Reducing (SAFER) Barriers, foams are located in a trapezoidal shape between steel and existing concrete wall as seen in Figure 1.3. Even though this easy and low cost solution, absorbed energy is increased dramatically [5].

Figure 1.4 A Typical Helmet [6]

Helmet designs are one of the main uses of foam. While helmets must have superior energy absorption performance against impact loads, they must have a lightweight design to place as little load on the driver's or pilot's neck as possible. In Figure 1.4, main parts of typical helmet are given and it is seen that crushable foam is used as liner foam to protect the wearer from impacts.

When a passenger aircraft takes off or lands, it can overshoot the available runway space. This can lead to accidents that result in aircraft damage and fatalities. In order to reduce the risk of aircraft overshooting, crash-landing systems are often installed at the ends of the runway. These crash-landing foam arrestor beds are designed to compress the aircraft tires as they roll through the foam. The compaction of the foam dissipates the energy of the aircraft, bringing it to a controlled landing. The current arrestor technology for civil aircraft uses a large, crushable bed of foam. The Federal Aviation Administration (FAA) designates this arrestor concept as an engineered material arresting system (EMAS). [7]

Figure 1.5 Crushable Foam Wrap [8]

Crushable foams are also used in oil well casing (Figure 1.5), where heat is generated as a result of drilling and production activities. As the temperature increases, the fluids trapped in the casing annulus tend to expand, potentially resulting in a high-pressure build-up. The most effective way to mitigate this build-up is to use crushable foam wrap, which allows the fluid to expand before the crushing occurs, thus preventing the formation of a potentially hazardous pressure. [9]

1.4. Scope of Thesis

The scope of thesis is investigating of accurate finite element model of crushable foam which will be used in flyer helmet as an energy absorber liner. The requirements of flyer helmet are determined according to MIL-DTL87174A design specification document. In pre-design stage of helmet, obtaining valid finite element model has a critical role on determining geometry and making lightweight design. To achieve this goal, experimental validation will be performed after understanding energy absorbing mechanism of foam and exploring finite element variations of crushable foam.

2. LITERATURE SURVEY

Halder and Sambamoorthy [10] studied appropriate material model selection of foam since it is difficult material to simulate because of its inherent unpredictability. It is crucial to know which material model is matching for a given kind of foam.

Liu et al [11] investigated a methodology to determine stress-strain curves of polymeric structural foams which are not initially available. In this study, two-step or multi-step uniaxial-strain compression is applied on foam to obtain crushability and residual crushability foam at different porosity levels.

Slik et al [12] proposed material modelling of IMPAXX^{TM} (crushable foam) with MAT 57 and MAT 63 material cards of LS-Dyna. Both resulting material models were showed good correlation against several type of tests which are pelvic shaped and head impact tests, drop tower simulations.

Croop and Lobo [1] studied appropriate material modelling for different types of foam. In this study, they worked on polyurethane foam, expanded polyethylene foam and expanded polystyrene foam by using 3 different types of LS DYNA material model cards which are MAT_LOW_DENSITY_FOAM (MAT57), MAT_CRUSHABLE_FOAM (MAT63), MAT_FU_CHANG (MAT83).

Ozturk and Anlas [13] presented a comparison between LS DYNA and ABAQUS about finite element simulation of foam under multiple compressive loading and unloading. They claimed that LS DYNA gives more accurate results although unloading simulation of LS DYNA should be improved. As an important note from this study, Ozturk and Anlas showed that stress-strain curve of crushable foams can be taken as strain rate independent after a certain deformation speed.

Shah and Topa [14] proposed the trial and error method to investigate shear failure criteria of EPS. Initially, they performed quasi-static compression test to determine stress-strain curve of expanded polystyrene at low strain rates. Then, gravity-driven drop tests were performed with semispherical impactor that penetrated to EPS. In drop tests, the brittle failure of EPS block was observed because of shear loads. In LS Dyna simulation,

ADD_EROSION and MAT_CRUSHABLE_FOAM material model applied. Comparing the depth of penetration in the drop test, simulation material parameters are developed by trial and error method.

Caliskan and Apalak [15] studied low velocity impact response of energy absorption panel which made of aluminum 6061-T6 and EPS foams had different densities. During the study, they analyzed EPS50, EPS100 and EPS180 under different energy levels with hemispherical impactor. As a result of the study, they noted that not much difference in impact behavior observed between different foam core densities.

W.Chen et al [16] investigated dynamic and static compressive behavior of EPS with density 13.5 kg/m^3 and $28kg/m^3$. They observed the dynamic strengths, energy absorption capacities and Young's module of two EPS foams which have different densities for different strain rates. They noted that Young's Modulus of EPS is remains almost constant with increasing strain rate.

G.C. Machado et al [17] proposed polymeric crushable foam model using the element free-Galerkin method. This elasto-plastic foam model is rate independent and includes a single surface yield criterion. This model was tested and showed reasonable predictions for the monotonic loading conditions.

Zhang et al [18] studied quasi static and dynamic indentation of a ball to different type of EPS foam blocks. They used EPS with density 9 kg/m^3, 13 kg/m^3 and 18 kg/m^3 to investigate indentation response of polystyrene foam. Also, during the finite element analysis, they modelled EPS by MAT57 material card of LS Dyna on the purpose of observing unloading effects of foam.

Ramon and Miltz [19] studied prediction of cushioning curves of foams from constant strain rate measurements. They compared the free-fall drop test and calculation results for semiflexible polyurethane with three different densities, expanded polystyrene and crosslinked polyethylene foams. According to these comparisons, they presented that cushioning curves of foams can be successfully determined using single stress-strain curve and their dynamic model, especially for EPS which is noticed as dynamically strain rate independent foam by them.

3. ENERGY ABSORPTION APPLICATION OF FOAM

3.1. Numerical Representation of Foam

Since impact protection must absorb kinetic energy while keeping peak stress below the injury or damage threshold, absorption material properties should be suitable for this mission. As mentioned before, foams perfectly fit for energy absorption applications for their unique material properties such as ease of application, lightweight, low cost and unique behavior under compression.

First of all, direction of impact is unpredictable and foams (roughly isotropic) can absorb energy in any direction in a cheap way. Also, they have capacity to undergo large deformation at constant stress. This property gives foam an excellent energy absorption capacity with little increase in stress. Foams always absorb more energy than solid for a determined peak stress.

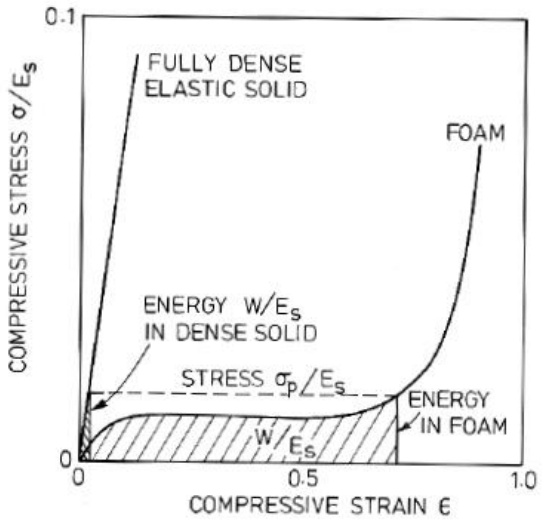

Figure 3.1 Stress Strain Curve Comparison of Foam and Solid [20]

Area under the stress-strain curve gives total amount of absorbed energy. As seen from Figure 3.1, energy increases along to stress plateau with little increase in peak stress. Then, peak stress increases sharply while absorbed energy remains constant when foam densifies. So that, optimum foams should be designed to absorb all of impact energy just before it densifies.

Stress strain curves of foam can be examined in two sections which are open cell foams and closed cell foams. Closed cell foams characteristics is more complicated than open cell foams. The reason of that fluid within cells is omitted for open cell foams since fluid flow dissipation does not affect the stress strain curve of foam unless fluid is viscous or rates are high. On the other hand, fluid within cells has a significant role on characteristics of closed cell foam.

In the following sections, given constants are designated according to best line of empirical values. In several cases, empirical results vary widely with respect to best line of overall results. Nonetheless, general behavior of foams has been determined in terms of several variables.

3.1.1. Compressive Stress Strain Curve of Open Cell Foams

Stress strain curves of open cell foams are investigated in several regimes and these regimes' behaviors can be varied depending on matrix material of foam. Compressive stress strain curves of open cell foams have 3 divided sections. First section is linear elastic and it corresponds to bending of the cell walls. Second section is stress plateau which ends with cell collapse. The stress plateau section of the compressive stress strain curve corresponds to buckling for elastomeric foams, plastic hinges for metallic foams and crushing for brittle foams. As a final section, densification occurs for all material types when every cell has been collapsed.

3.1.1.1. Linear Elastic Behavior

Considering a cubic cell with a square cross section member of area t^2 and length l, linear elasticity occurs due to bending of the cell walls since thickness of the cell edges is relatively small to the length of cubic cell element. If thickness to length ratio gets higher, axial deformation becomes more significant for this section of stress strain curve.

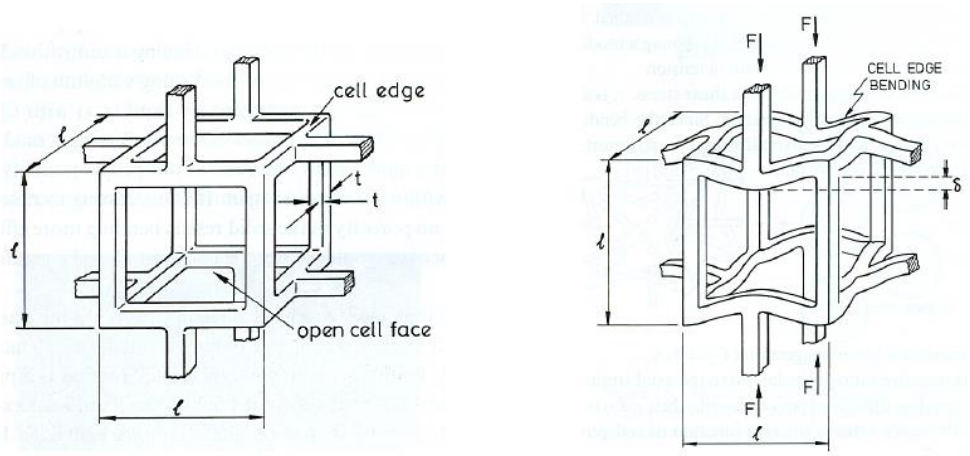

Figure 3.2 Cubic Open Cell Element Representation [20]

Relative density of foam is equal to volume fraction of the solid in the foam. Also, the moment of inertia of square cross section area is related to t^4 since $b = h$ for square.

$$\frac{\rho^*}{\rho_s} = \frac{V_s}{V_T} \propto \frac{t^2 l}{l^3} \propto (t/l)^2 \tag{3.1}$$

$$I \propto t^4 \tag{3.2}$$

As seen from Figure 3.2 stress, strain and displacement relations can be written as:

$$\sigma \propto F/l^2 \tag{3.3}$$

$$\varepsilon \propto \delta/l \tag{3.4}$$

$$\delta \propto \frac{Fl^3}{E_S I} \tag{3.5}$$

By merging these relations, modulus of a foam can be found:

$$\delta \propto \frac{Fl^3}{E_S I} \tag{3.6}$$

$$E^* = C_1 E_s (\rho^*/\rho_s)^2 \tag{3.7}$$

Where C_1 includes all geometrical constants and can be taken as 1 according to experimental data. Since full scale structural analysis of tetrakaidekahedron cell shows that $C_1 = 0.98$. As seen from Figure 3.3, tetrakaidekahedron unit cell geometry has the varying thickness along the edge [20]. Therefore, geometrical constants can be ignored even tetrakaidekahedron unit cell has 0.98 geometrical constant value.

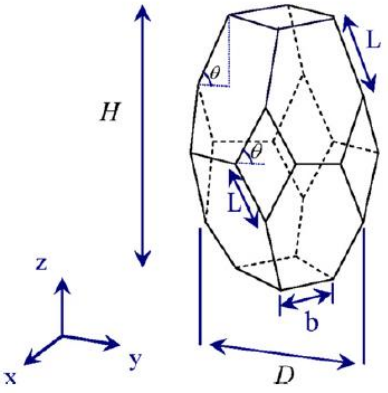

Figure 3.3 Tetrakaidekahedron Unit Cell Representation [21]

$$E^* = E_s(\rho^*/\rho_s)^2 \tag{3.8}$$

Shear modulus of open cell foam:

$$G^* = C_2 E_s(\rho^*/\rho_s)^2 \tag{3.9}$$

C_2 can be taken as $3/8$ for isotropic foams. Also, Poisson's ratio of isotropic foam can be taken as constant which depends on only geometry of cell.

$$G = \frac{E}{2(1+\nu)} \tag{3.10}$$

$$\nu^* = \frac{E}{2G} - 1 = \frac{C_1}{2C_2} - 1 = C_3 \tag{3.11}$$

3.1.1.2. Non-Linear Elastic Behavior

In open cell foams, elastic collapse stress occurs due to cell wall buckling. So that, buckling load can calculate by usual Euler's load equation. Elastic buckling stress relations can be written as:

$$P_{cr} = \frac{n^2 \pi^2 E_s I}{l^2} \tag{3.12}$$

$$\sigma_{el} \propto \frac{P_{cr}}{l^2} \propto E_s \left(\frac{t}{l}\right)^4 \tag{3.13}$$

By using (3.1) and (3.8) elastic buckling stress can be shown as:

$$\sigma_{el}^* = C_4 E_s \left(\frac{\rho^*}{\rho_s}\right)^2 \tag{3.14}$$

Empirical data presents that $C_4 \approx 0.05$, corresponds to strain at which buckling occurs since remaining of the equation represents Young's Modulus of foam as mentioned in Equation (3.8).

3.1.1.3. Plastic Collapse Strength

Plastic collapse is observed in metallic and rigid polymer foams and occurs when applied moment equals to plastic moment. Also, plastic collapse is preceded by elastic collapse. However, it is impossible in rigid polymers and metals since critical relative densities of these are far away from the boundary.

- Plastic moment relevance:

$$M_p \propto \sigma_{ys} t^3 \tag{3.15}$$

- Applied moment relevance:

$$M \propto \sigma_{pl}^* l^3 \tag{3.16}$$

$$\sigma_{pl}^{*} = C_5 \sigma_{ys} (\rho^{*}/\rho_s)^{3/2} \quad (3.17)$$

Empirical data presents that $C_5 \approx 0.05$. [20]

$$\sigma_{pl}^{*} = 0.05 \sigma_{ys} (\rho^{*}/\rho_s)^{3/2} \quad (3.18)$$

3.1.1.4. Brittle Crushing Strength

Brittle crushing is observed in brittle foams like ceramic and occurs when applied moment equals to fracture moment.

- Fracture moment relevance:

$$M_f \propto \sigma_{fs} t^3 \quad (3.19)$$

- Applied moment relevance:

$$M \propto \sigma_{cr} l^2 \quad (3.20)$$

$$\sigma_{cr} = C_6 \sigma_{fs} (\rho^{*}/\rho_s)^{3/2} \quad (3.21)$$

Empirical data presents that $C_6 \approx 0.2$. [20]

$$\sigma_{cr} = 0.2 \sigma_{fs} (\rho^{*}/\rho_s)^{3/2} \quad (3.22)$$

At very large strains, cell walls begin to touch each other which causes that stress rises sharply at densification strain. At that point, modulus of foam becomes equal to modulus of solid. Empirical result of the densification strain for both open and closed cell foams is:

$$\varepsilon_D = 1 - 1.4 \rho^{*}/\rho_s \quad (3.23)$$

3.1.2. Compressive Stress Strain Curve of Closed Cell Foams

Stress strain curves of closed cell foams have same regimes with open cell foams. The difference between them is cell faces and containing liquid. These differences affect required stress level at the same strain for same matrix material. In other words, the closed cell foams absorb more energy than open cell foams for the same material and density.

3.1.2.1. Linear Elastic Behavior

In linear elastic regime, closed cell foams absorb energy by edge bending, face stretching and gas compression while open cell foams absorb energy only by edge bending.

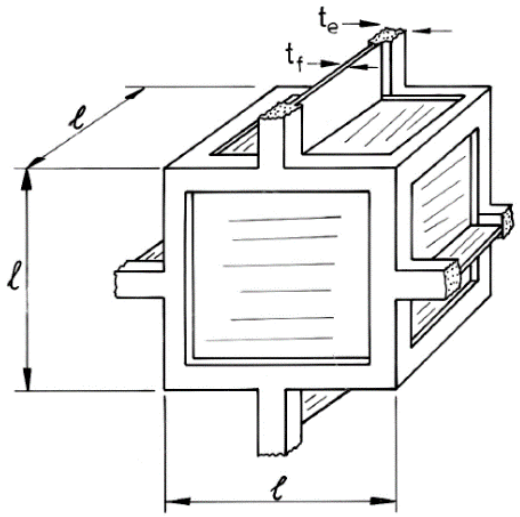

Figure 3.4 Cubic Closed Cell Element Representation [20]

External work done by applying axial force has to be equal to internal work done by edges bending and faces stretching while gas compression. Their relations can be written as by using geometrical parameters given in Figure 3.4:

- External work done:

$$\propto F\delta \tag{3.24}$$

- Internal work done by bending edges due to their stiffness:

$$\propto \frac{F_e}{\delta_e}\delta_e^2 \propto \frac{E_s I}{l^3}\delta^2 \tag{3.25}$$

- Internal work done from stretching faces in terms of Hook's Law:

$$\propto \sigma_f \varepsilon_f v_f \propto E_s \varepsilon_f^2 v_f \propto E_s(\delta/l)^2 t_f l^2 \tag{3.26}$$

- Also, modulus of the foam is related to by using Equation (3.3) and (3.4):

$$E^* \propto \frac{F}{l^2}\frac{l}{\delta} \rightarrow F \propto E^*\delta l \tag{3.27}$$

By balancing internal work to external work:

$$F\delta = \alpha \frac{E_s t_e^4}{l^3}\delta^2 + \beta E_s \left(\frac{\delta}{l}\right)^2 t_f l^2 \tag{3.28}$$

$$E^*\delta^2 l = \alpha \frac{E_s t_e^4}{l^3}\delta^2 + \beta E_s \left(\frac{\delta}{l}\right)^2 t_f l^2 \tag{3.29}$$

$$E^* = \alpha E_s \left(\frac{t_e}{l}\right)^4 + \beta E_s \left(\frac{t_f}{l}\right) \tag{3.30}$$

Different from the Equation (3.1) relative density for closed cells with uniform thickness is related to:

$$\frac{\rho^*}{\rho_s} = \frac{V_s}{V_T} \propto \frac{tl^2}{l^3} \propto (t/l) \tag{3.31}$$

And, if φ is taken as volume fraction of solid in cell edges Equation (3.30) becomes:

$$\frac{E^*}{E_s} = C_1\varphi^2(\rho^*/\rho_s)^2 + C_1'(1-\varphi)\rho^*/\rho_s \tag{3.32}$$

Since

$$t_e/l = C\varphi^{1/2}(\rho^*/\rho_s)^{1/2} \tag{3.33}$$

$$t_f/l = C'(1-\varphi)(\rho^*/\rho_s) \tag{3.34}$$

As mentioned before, containing gas also contribute to modulus of closed cell foams. For cubic element of foam which has volume V_0 and deformed volume V with axial strain ε:

$$V_0 = l_0^3 \tag{3.35}$$

$$V = l_1 l_2 l_3 \tag{3.36}$$

$$\varepsilon_1 = \frac{l_1 - l_0}{l_0} \rightarrow l_1 = l_0 + \varepsilon_1 l_0 = l_0(1+\varepsilon_1) \tag{3.37}$$

$$\varepsilon_2 = -\nu\varepsilon_1 \tag{3.38}$$

$$\varepsilon_2 = \frac{l_2 - l_0}{l_0} \rightarrow l_2 = l_0 + \varepsilon_2 l_0 = l_0 - \nu\varepsilon_1 l_0 = l_0(1-\nu\varepsilon_1) \tag{3.39}$$

$$\varepsilon_3 = l_0(1-\nu\varepsilon_1) \tag{3.40}$$

$$\begin{aligned} V = l_1 l_2 l_3 &= l_0(1+\varepsilon_1) l_0(1-\nu\varepsilon_1) l_0(1-\nu\varepsilon_1) \\ &= l_0^3(1+\varepsilon_1)(1-\nu\varepsilon_1)^2 \end{aligned} \tag{3.41}$$

$$\frac{V}{V_0} = \frac{l_0^3(1+\varepsilon)(1-\nu\varepsilon)^2}{l_0^3} = (1+\varepsilon)(1-2\nu\varepsilon+\nu^2\varepsilon^2) \tag{3.42}$$

$$= (1-2\nu\varepsilon+\nu^2\varepsilon^2) + \varepsilon - 2\nu\varepsilon^2 + \nu^2\varepsilon^3 \tag{3.43}$$

Taking compression as positive and neglecting ε^2 and ε^3 terms, because they are relatively too small:

$$\frac{V}{V_0} = 1 - \varepsilon + 2\nu\varepsilon \tag{3.44}$$

$$\frac{V}{V_0} = 1 - \varepsilon(1 - 2\nu) \tag{3.45}$$

By extracting solid volume from total volume:

$$\frac{V_g}{V_g^0} = \frac{1 - \varepsilon(1 - 2\nu^*) - \rho^*/\rho_s}{1 - \rho^*/\rho_s} \tag{3.46}$$

From Boyle's Law:

$$pV_g = p_0 V_g^0 \tag{3.47}$$

$$p' = p - p_0 \tag{3.48}$$

$$p' = p - p_0 = \frac{p_0 V_g^0}{V_g} - p_0 = p_0 \left(\frac{V_g^0}{V_g} - 1 \right) \tag{3.49}$$

$$p' = \frac{p_0 \varepsilon(1 - 2\nu^*)}{1 - \varepsilon(1 - 2\nu^*) - \rho^*/\rho_s} \tag{3.50}$$

$$E_g^* = \frac{dp'}{d\varepsilon} = \frac{p_0(1 - 2\nu^*)}{1 - \rho^*/\rho_s} \tag{3.51}$$

Finally, modulus of closed cell foam becomes by containing edge bending, face stretching and gas compression:

$$\frac{E^*}{E_s} = \varphi^2 \left(\frac{\rho^*}{\rho_s} \right)^2 + (1 - \varphi) \left(\frac{\rho^*}{\rho_s} \right) + \frac{p_0(1 - 2\nu^*)}{E_s(1 - \rho^*/\rho_s)} \tag{3.52}$$

Also, shear modulus of isotropic closed cell foam which contributes edge bending and face stretching presented below. There is no gas compression term in shear modulus since volume change is equal to zero in shear.

$$\frac{\varepsilon^*}{E_s} = \frac{3}{8}\left[\varphi^2\left(\frac{\rho^*}{\rho_s}\right)^2 + (1-\varphi)\left(\frac{\rho^*}{\rho_s}\right)\right] \tag{3.53}$$

$$\frac{V}{V_0} = 1 - \varepsilon + 2\nu\varepsilon \tag{3.54}$$

3.1.2.2. Non-Linear Elastic Behavior

Thickness of the cell wall is very high when compared to face thickness as seen from Figure 3.4. Due to that reason, contribution of faces to compressive buckling strength is negligible. However, there can be contribution from the internal pressure if internal pressure is greater than atmospheric pressure. In that case, cell walls are pretensioned and buckling stress should overcome this pretension. So that, elastic buckling stress for closed cell foams can be written by summing elastic buckling stress for open cell foams and contribution from the internal pressure:

$$\sigma_{el}^* = C_4 E_s\left(\frac{\rho^*}{\rho_s}\right)^2 + p_0 - p_{atm} \tag{3.55}$$

$$\sigma_{el}^* = 0.05 E_s\left(\frac{\rho^*}{\rho_s}\right)^2 + p_0 - p_{atm} \tag{3.56}$$

As a difference from open cell foams, stress plateau rises because of gas compression after cell wall collapse if faces do not rupture. Also, Poisson's ratio of closed cell foams are equal to zero ($\nu^* = 0$) at that regime due to gas compression. Because they are not getting wider after the buckling occurs. By using Equation (3.50) in (3.56), post collapse stress of closed cell foam can be written as:

$$\sigma_{post-collapse}^* = 0.05 E_s\left(\frac{\rho^*}{\rho_s}\right)^2 + \frac{p_0\varepsilon}{1-\varepsilon-\rho^*/\rho_s} \tag{3.57}$$

3.1.2.3. Plastic Collapse Strength

Theoretically, plastic collapse stress of closed cell foam can be written as:

$$\sigma_{pl}^{*} = C_5\sigma_{ys}\left(\varphi\frac{\rho^{*}}{\rho_s}\right)^{3/2} + C_5'\sigma_{ys}(1-\varphi)\left(\frac{\rho^{*}}{\rho_s}\right) + p_0 - p_{atm} \qquad (3.58)$$

In practice, faces of cell often rupture around σ_{pl}^{*} so that plastic collapse stress of closed cell foam becomes same as open cell foams stress. Because of this, plastic collapse stress of closed cell foam can be written as presented in Equation (3.18):

$$\sigma_{pl}^{*} = 0.05\sigma_{ys}(\rho^{*}/\rho_s)^{3/2} \qquad (3.59)$$

3.1.2.4. Brittle Crushing Strength

Brittle crushing strength is similar to plastic collapse strength of closed cell foams and it can be given as:

$$\sigma_{cr}^{*} = C_6\sigma_{fs}\left(\varphi\frac{\rho^{*}}{\rho_s}\right)^{3/2} + C_6'\sigma_{fs}(1-\varphi)\left(\frac{\rho^{*}}{\rho_s}\right) + p_0 - p_{atm} \qquad (3.60)$$

As provided in Equation (3.22) C_6 and C_6' can be taken as 0.2 and 1, respectively according to empirical data. Since brittle crushing strength of closed cell foam cannot be obtained exactly by Equation (3.60), the dependence of the strength on density can be predetermined. Therefore, as the solid fraction in the cell faces increases, membrane stress becomes dominant. Due to that reason, strength dependence on density is reformed as linear instead of power of $3/2$.

3.2. Energy Absorption Requirements for Helmets

The primary focus of many helmet standards is impact protection. While shock absorption tests are the general term for tests to evaluate impact protection, helmet quality isn't measured by measuring the amount of energy absorbed. Instead, an acceleration time history is measured for a helmeted headform during an impact. This history is used to determine injury parameters, such as maximum acceleration in the headform, as well as

other criteria related to the potential for injury. The severity of the test depends on the test conditions and requirements for the headform and helmet prior to impact, as well as the anvil shape. There are four different impact anvils: the flat one used in all standards, the hemispherical, the kerbstone and the edge.

Table 3.1 Acceptance criteria for helmet safety standards [22]

Standard	**Criterion**
Snell M2000	$a_{max} < 300$ [g]
DOT FMVSS 218	$a_{max} < 400$ [g] $a_{[2ms]} < 200$ [g] $a_{[4ms]} < 100$ [g]
ECE 22	$a_{max} < 275$ [g]

Maximum acceleration in the headform is often used parameter as head injury criterion. Acceptable maximum acceleration varies depending on application, since head injury is time dependent to resultant acceleration as stated at Wayne State Tolerance Curve (WSTC) which is given in Figure 3.5. WSTC is regarded as the primary source for research on the head injury criteria and the majority of currently recognized injury criteria are still based on WSTC.

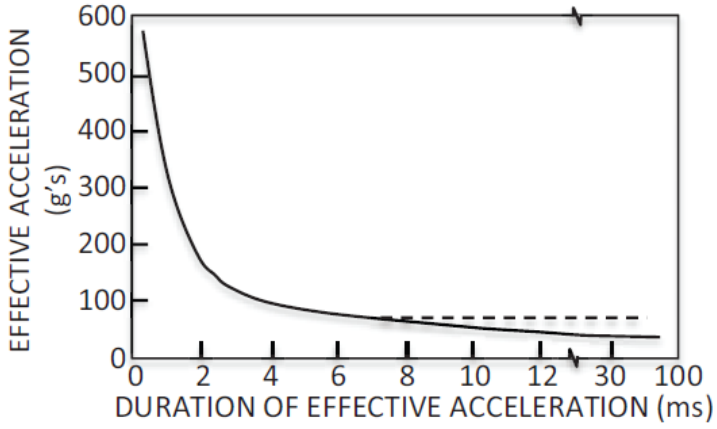

Figure 3.5 Wayne State Tolerance Curve [23]

3.2.1. Snell M2000 Standard for Protective Headgear

M2000 requires a minimum of 5 impacts on a single helmet in the following sequence: Two impacts at a single site by using flat anvil, two impacts by using hemispheric anvil at a site at a minimum of 120 mm away from the previous site, one impact on an edge anvil at a minimum distance of 120 mm off the previous ones. The impact severity is expressed in terms of kinetic energy of falling headform/headform guidance system without the helmet. Headform mass does not change with headform size. The first drop will always be 150 J, equivalent to a 7.7m/s impact, and if required the second drop will always be 110 J, equivalent to a 6.6m/s impact. The impact procedures leave a significant amount of flexibility to the helmet tester regarding the impact site and the choice of anvil. It is expected that the tester will utilize his experience to organize each test series so that potential weaknesses and probable failure modes are exploited. [22]

3.2.2. DOT FMVSS218 Helmet Safety Standard

According to the DOT standard, each helmet receives 8 impacts, two on each anvil (flat and hemispherical), at each site. The impact sites shall be at least one-sixth of the circumference of the headform. The severity is described by headform velocity just before impact. The velocity is dependent on the anvil, but it is equal for the first and second impact. However, the kinetic energy before impact is different for all headforms, since a large headform including guidance system is heavier than a small one with guidance system. The helmet size also determines the headform and therefore the kinetic energy of both the headform and the headform guidance system before impact. The kinetic energies before impact for the small, medium, and large headform including the guidance system are 63, 90, and 110 J, respectively for the flat anvil test while they are 47, 68, and 82 J for the hemispheric anvil test. [22]

3.2.3. UN Regulation No.22 (ECE 22)

In the ECE standard, only single impacts are required against the flat and kerstone anvils, and just like DOT, the impact severity is described by the impact velocity: 7.5 m/s for both anvils. The ECE standard uses eight different sized ISO headforms which are A, C, E, E, G, J, K, M and O types. E, J & M ISO headforms are can be considered as small, medium and large DOT headforms, respectively. Impact energies of these headforms are

115, 132 & 158 J, respectively. The single impact level of the ECE standard is close to the first impact level of the M2000, and even exceeds it for large size headforms. Impact sites for the ECE standard are predetermined which are front, side, top & rear of helmet. [22]

3.2.4. MIL-DTL-87174A

MIL-DTL-87174A is detail specification document which covers the HGU-55/P flyer's helmet requirements. In this military specification document, impact protection test procedure is based on ANSI Z90.1 (Headgear Protective for Motor Vehicular Users Specifications for) with several changes. According to MIL-DTL-87174A, each helmet shall be subjected 5 impacts only with rigid hemispherical impactor. These impacts have 35 foot-pound impact energy and applied to the front, back, crown and both side locations. The acceleration of headform is limited by 400g. Also, the recorded acceleration shall not exceed 150g for more than 6 milliseconds and 200g for 3 milliseconds.[24]

Additionally, the detail specification document determines energy absorber liners' material as EPS having a density of 2 – 2.5 pounds per cubic foot (32.04 – 40.05 kilograms per cubic meter). [24]

3.3. Strain Rate Effect

Together with the complex structure of foam, strain rate effect is another reason to difficulty of foam modelling. Stress strain curve of structural foams shifts up by increasing strain rate. In addition, strain rate dependence is not proportional for all kind of foam. It is observed that, stress at densification strain is proportional to logarithm of strain rate for open cell elastomeric foams. As an example, graph of flexible polyurethane normalized energy per unit volume vs. normalized peak stress for different strain rates is given in Figure 3.6. Shoulder points which describes where peak stress begin to increase sharply. It is observed that shoulder points of each flexible polyurethane have a linear slope in logarithmic scale for given strain rates which are logarithmically linear. On the other hand, it is very difficult to observe similar relation for other type of structural foams especially for closed cell foams.

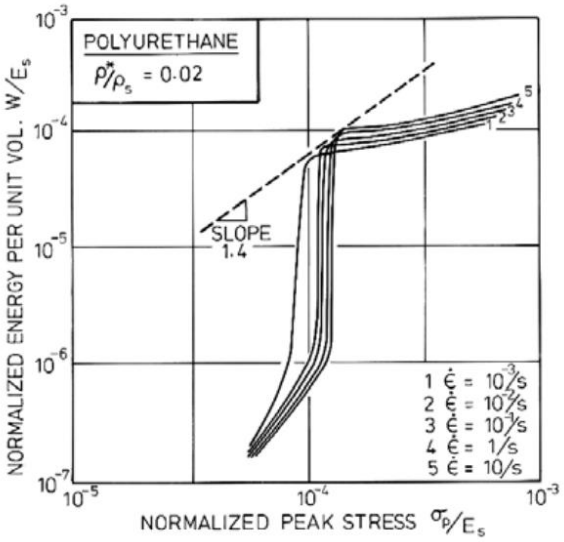

Figure 3.6 Flexible Polyurethane Normalized Energy per Unit Volume vs. Normalized Peak Stress for Different Strain Rates [20]

Since linear elastic behavior is solid material dominated for open and closed cell foams, the Young's Modulus of foam is independent of the strain rate. It is only dependent on normalized density of solid as seen in Equation (3.7) and (3.52). In the study of Chen et al. [16] several experiments were performed to obtain dynamic mechanical properties of EPS and they showed that Young's Modulus of EPS is not strain rate sensitive. Also, Zhang et al. [18] achieved same results and underlined that modulus of EPS is only foam density dependent.

To determine stress strain curve of EPS35 at different strain rates, several experiments were conducted by ASELSAN. In these experiments, cylindrical EPS35 specimens with $60mm$ diameter and $25mm$ height were compressed according to ASTM D1621 by DARTEC uniaxial compression machine which is presented in Figure 3.7.

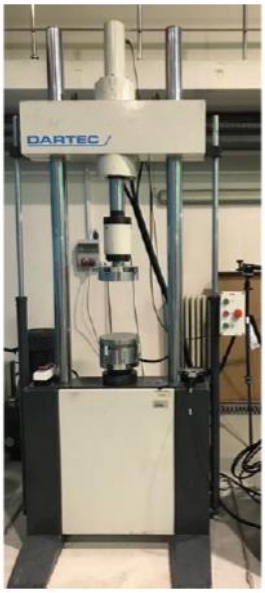

Figure 3.7 DARTEC Uniaxial Compression Machine

Compression speeds of experiments were $2mm/min$, $3000mm/min$ and $3500mm/min$. Therefore, strain rates of experiments were $1.33x10^{-3}, 2, 2.33\ {}^{1}/_{s}$, respectively. Experiments were performed 5 times for each speed until 92% strain and stress strain curves of EPS35 were perfectly matched for individual strain rates. The reason of $3500mm/min$ choice is the highest achievable compression speed by DARTEC. As a result of these compression test, strain rate effect on EPS35 were observed. Comparison of stress strain curves presented in Figure 3.8.

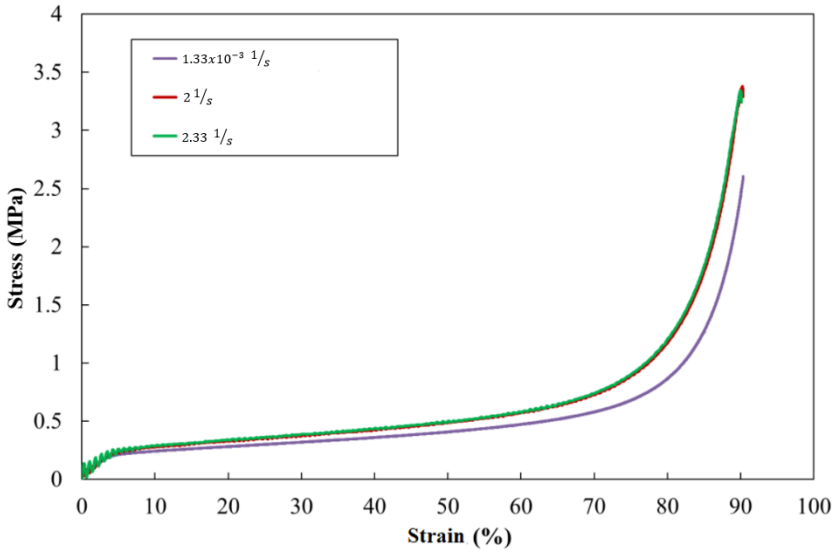

Figure 3.8 Stress Strain curves of EPS35 at different compression speeds

As seen from Figure 3.8, there is no significant difference in Young's Modulus and behavior of EPS. On the other hand, stress values are shifted up by increasing strain rate.

There are several experimental studies in literature about strain rate dependency of stress strain curve of EPS materials. For instance, Ramon and Miltz [19] modeled EPS dynamically strain rate independent. Also, Zwang et al. [25] observed that stress-strain curve of crushable foams can be taken as not strain rate dependent after a certain deformation speed as mentioned before. In the study, they performed uniaxial compression test at four different strain rates until 80% strain and compared the results with their strain rate sensitivity characterization model.

$$\sigma(\varepsilon) = \sigma_0(\dot{\varepsilon}/\dot{\varepsilon}_0)^{n(\varepsilon)} \tag{3.61}$$

$$n(\varepsilon) = a + b\varepsilon \tag{3.62}$$

The EPS sample dimensions were $50x50x50mm^3$, and compression speeds were $8x10^{-5}, 4x10^{-3}, 0.229$ and $4.45\, m/s$. Corresponding strain rate values for these compression speeds are $1.60x10^{-3}, 8x10^{-2}, 4.58$ and $8.90x10^{1}\ 1/s$, respectively. As seen from results of experiments that are provided below, the difference between stress levels of $4x10^{-3}\ m/s$ ($8x10^{-2}\ 1/s$) and $4.45\, m/s$ ($8.90x10^{1}\ 1/s$) is less than 10% for EPS80 ($1.6\ kg\ m/mm^3$ is equal to $80\ kg/m^3$ for $50mm$ height). So that, $2.33\ 1/s$ strain rate results can be used for material model validation studies even if it is considerably lower than impact speed.

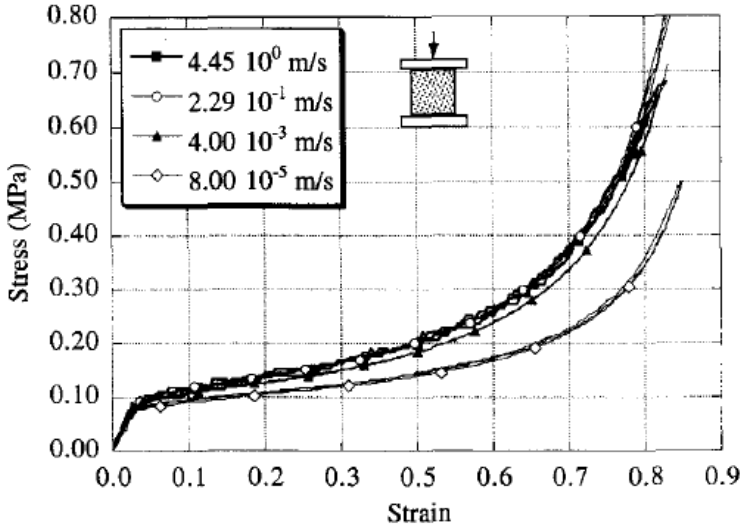

Figure 3.9 Stress Strain curves of EPS (density 1.6 kg m/mm^3) at different compression speeds [25]

4. FINITE ELEMENT MODEL OF THE FOAM

To simulate difficult real-world issues LS-Dyna module embedded in ANSYS Workbench 2023R2 is chosen as a nonlinear finite element program in this thesis. As mentioned before, Ozturk and Anlas [13] presented that LS-Dyna gives more accurate results than ABAQUS at impact analysis of crushable foams. Apart from accuracy of results, LS-Dyna has several advantages such that the code includes mature contact treatments, low memory requirements, a variety of material models, and affordable time-step calculations.

LS-Dyna was first used in 1976 under the name DYNA3D at the Lawrence Livermore National Laboratory, the code's primary areas of interest are highly nonlinear and transient dynamic finite element analyses. The code's initial use is in the stress analysis of structures that are exposed to various impacts.

Based on the approach taken to solve the problem, explicit codes and static, structural dynamic codes differ fundamentally. A dynamic model needs to be solved for every time step, as opposed to a static model, which can be solved for a limited number of load steps. The time step in an explicit dynamic code can be as short as one microsecond and is determined by how long it takes a sound wave to travel across the smallest element.

LS-DYNA is a central difference method explicit code. For the system to be stable, the time step size must be smaller than its maximum frequency.

4.1. Finite Element Material Models of Foam in LS-Dyna

Due to foams' wide usage application areas, foams with significantly varied characteristics which meet individually to end use needs has been developed. Because of that, there are several foam material cards investigated in LS-Dyna. To create meaningful finite element model, using appropriate material model card has a significant role. In this section of thesis, these material model cards are introduced briefly.

Table 4.1 Foam Material Cards [26]

MATERIAL CARD ID	DESCRIPTION
MAT_005	Relatively simple material model for crushable foam
MAT_014	Used only when foams are confined within a structure and pressure reaches tensile failure pressure.
MAT_026	Used for anisotropic honeycomb and foam materials. Nonlinear elastoplastic material behavior can be defined.
MAT_038	Used for the definition rubber like polyurethane foams
MAT_053	Used for closed cell polyurethane foams with low density
MAT_057	Used for highly compressible foam with low density
MAT_061	Used for modelling viscoelastic bodies by using Kelvin-Maxwell model
MAT_062	Represents Confor Foam on the EuroSID side impact dummy
MAT_063	Used for modelling crushable foam with optional damping, unloading is elastic in this model
MAT_073	Used for modelling urethane foam with low density
MAT_075	Used for modelling isotropic crushable foam with triaxial test data
MAT_083	Used for modelling low and medium density foam with strain rate dependency
MAT_142	Used for simulate the extruded crushable low-density foam material which is transversely isotropic with no significant Poisson effect.
MAT_144	Used for modelling isotropic crushable foam with strain rate effects
MAT_154	Used for simulate aluminum foams

MAT_163	Modified version of MAT_063, this model includes strain rate effects
MAT_177	Used for modelling highly compressible foam in terms of strain-energy function
MAT_178	Used for modelling highly compressible foam in terms of strain-energy function
MAT_179	Used for simulate loading-unloading behavior of rate independent low-density foams
MAT_180	Used for simulate loading-unloading behavior of rate independent low-density orthotropic foams
MAT_181	Relatively simple material model for rubber and foam

In this study, MAT_057 and MAT_063 are chosen as material cards as the most suitable ones to situation. MAT_057 material card is created to simulate highly compressible low-density foams. On the other hand, MAT_063 is developed for modelling crushable foams that have completely elastic unloading curve.

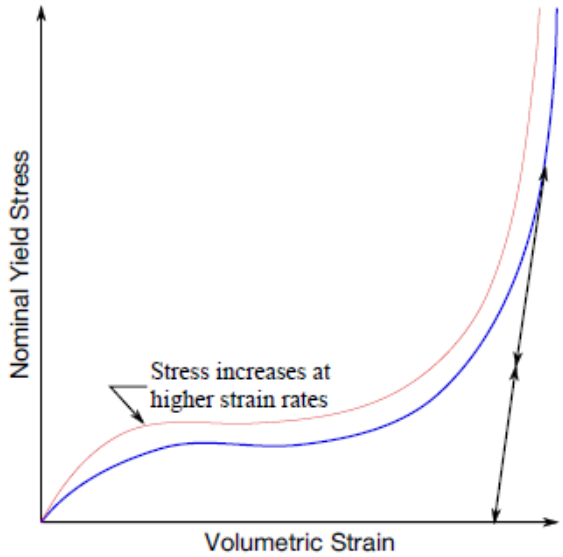

Figure 4.1 Behavior of strain rate sensitive crushable foam and unloading curve of MAT_063 [26]

MAT_063 depends on von Mises yield condition and in this material card, load curve defines yield stress as a function of volumetric strain. As mentioned in Section 3.1.2.2, Poisson's ratio of closed cell foams are equal to zero at non-linear elastic regime since gas compression. MAT_063 material model card is suitable for EPS due to volumetric strain is equal to uniaxial strain when Poisson Ratio of material is equal to zero. Because

of that, crushable foam such as EPS can be modelled by using uniaxial strain data in LS-Dyna solver and their limited unloading behavior can also be observed since their unloading curve depends only on Young's Modulus of load curve and tension cut off value. Unloading curve of crushable foam material card is simulated as tangent to load curve as represented in Figure 4.1

There are several EPS modelling studies in the literature and these studies also presented that MAT_063 is accurate material card to analyze compression behavior of crushable foams. [1, 12, 14]

Before Compression Test

$2mm/min$ $3000mm/min$ $3500mm/min$

After Compression Test

Figure 4.2 Foam specimens before and after the uniaxial compression test

Although EPS is assumed to have limited unloading behavior in the literature, during the uniaxial compression experiments it is observed that it has considerably high unloading behavior at high strain rates as seen from Figure 4.2. Observation of unloading behavior

of foam is important, since duration over predefined acceleration values is another constrain of energy absorption standards beside the peak acceleration. MAT_057 is chosen as second material card since it has hysteresis upon unloading and simulation unloading behavior of foam. However, this material card simulates foam as fully recoverable as seen in Figure 4.3.

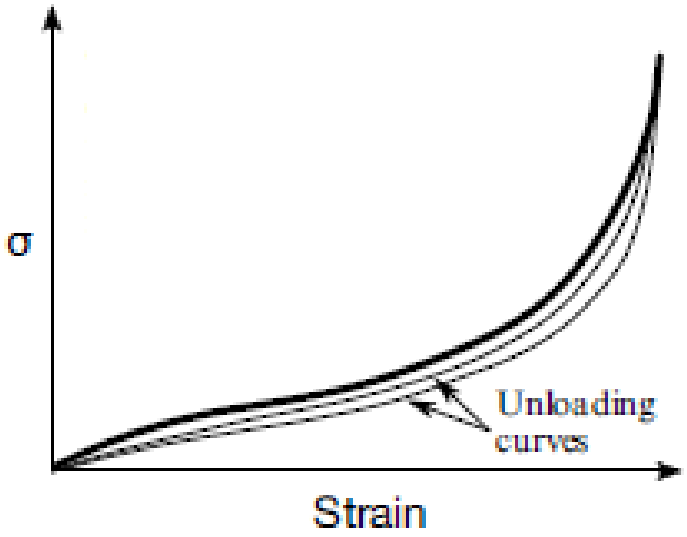

Figure 4.3 Behavior of low-density foam (MAT_057) [26]

There are also many studies which represent MAT_057 is accurate material card to observe loading and unloading behavior of EPS. [12, 13, 18]

4.2. Time Step

In fast process such as impact, explicit solvers are chosen to observe short time dynamics. In explicit analysis the equilibrium of equation of motion is set up for current time by Central Difference Method and explicit time integration method provides several advantages. The main reason of these advantages of explicit time integration method is that, there is no matrix inversion as a result of diagonal mass matrix, uncouple equations. Because of that, explicit analysis requires low memory and do not require any iteration or convergence. On the other hand, time step of explicit solver should be smaller than critical time step for stable solution.

In LS-Dyna, Courant Friedrich Levy (CFL) is used as time step criterion. Time step of analysis is determined by element with smallest time step since all finite elements have a time step. In addition, critical time step can vary during the analysis due to nonlinearities. According to CFL Time Step Criteria, critical time step should be less than travel duration of a sound wave to through an element. [27]

$$\Delta t \leq \frac{L}{c} \approx L\sqrt{\frac{\rho}{E}} \tag{4.1}$$

As seen from Equation (4.1), critical time step depends on element size and linear material properties for explicit analysis and LS Dyna uses 0.9 as a time scale factor by default. In addition, time scale factor can be changed by user to increase stability of solver in some cases.

4.3. Energy Considerations

For observing correctness of explicit analysis law of conservation of energy should be considered. In other words, total energy of the system must be the same unless there is no external effect.

LS Dyna uses reduced integration solid/shell elements by default due to several reasons which are CPU time saving in element processing, memory saving and avoiding locking problems. However, in some cases, these elements may require stabilization. These reduced integrated elements might be the reason of hourglass energy in some cases. For example, in impact analysis, hourglass energy control is the first thing in analysis setup. On the other hand, LS Dyna also provide fully integrated elements with more computational effort.

Hourglass energy is zero-energy modes of deformation that produce zero strain and no stress [28] and occurs only in 8 node hex solids and 4 node quad shell elements. To eliminate hourglass energy there are several methods. First of all, fully integrated 8 node hex elements could be used instead of reduced integrated element or artificial stiffness can be added to model or suitable hourglass control can be defined according to LS-Dyna Manual. There are 6 hourglass control options for solid elements. Also, 5 options are available for shell elements.

Hourglass energy can be monitorized from LS-Dyna's energy outputs or can be observed on mesh in some cases such as given example in Figure 4.4.

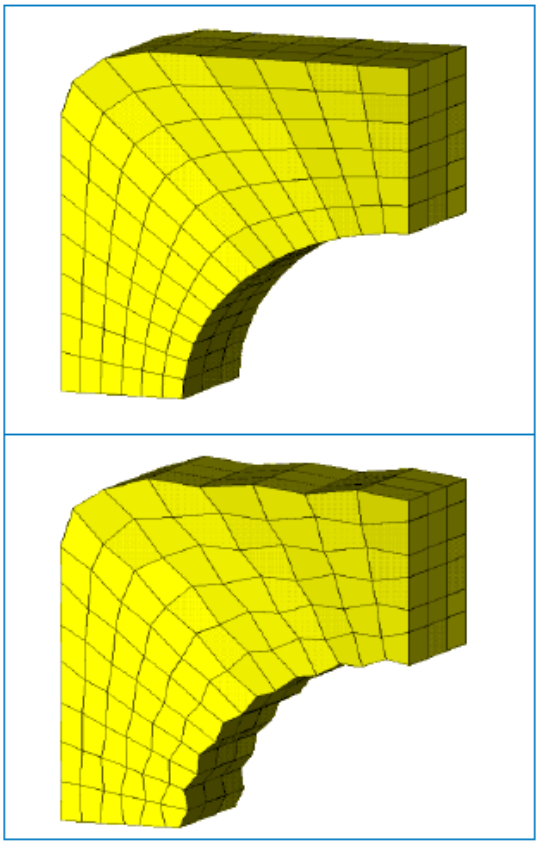

Figure 4.4 Hourglassing example [29]

Additionally, hourglass energy can be reduced or entirely eliminated by choosing appropriate element formulation. There is a tradeoff between hourglass energy reduction and computational effort and this tradeoff should also be considered depending on analysis model. Hourglass energy should not exceed 10% of internal energy as a rule of thumb. Apart from hourglass, conservation of energy should be checked in every case.

4.4. Finite Element Development Process

First of all, CAD model which corresponds to experimental setup was created by PTC Creo and its implemented to ANSYS Workbench 2023 R2 by using CAD integration. In experimental setup, geometry of EPS35 was determined such that it has $150mmx150mm$ cross section with different heights. To illustrate, cad model of analysis setup for 25mm height EPS35 is given in Figure 4.5.

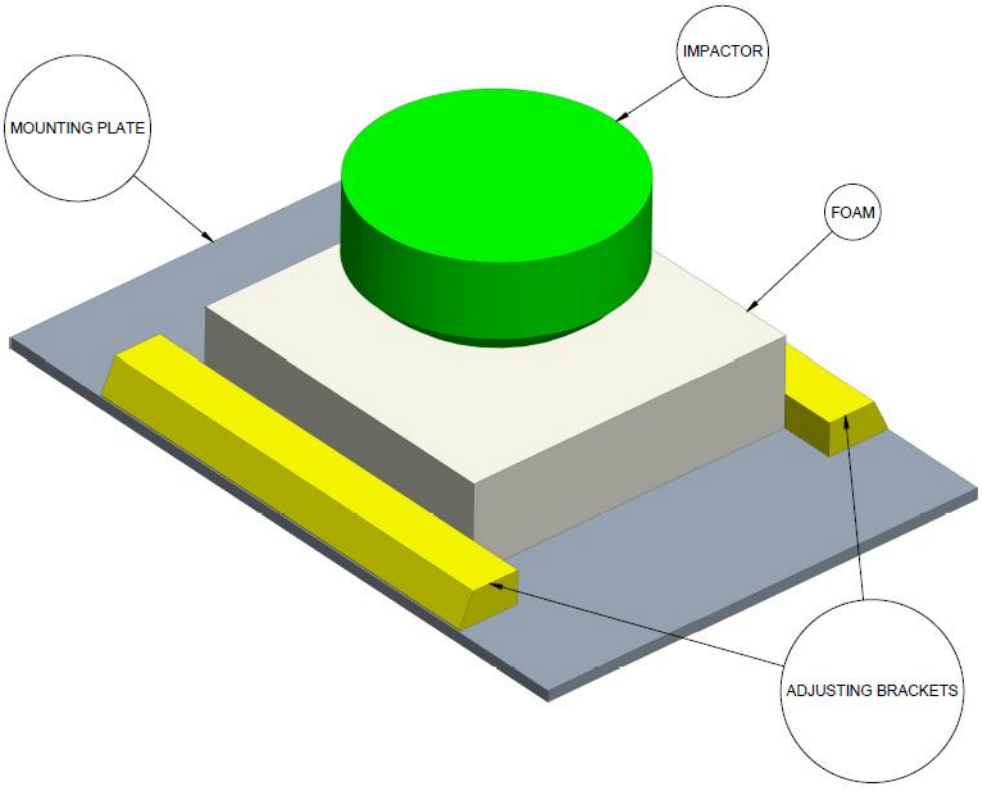

Figure 4.5 CAD Model of Analysis Setup for 25mm Height EPS35

After CAD model integration, engineering data was set and geometry properties were chosen. In engineering data setting, EPS35 material properties were defined by MAT_057 low-density foam and MAT_063 crushable foam material card of LS-Dyna due to reasons expressed in Section 4.1. EPS35 material card was created as expressed below:

Table 4.2 MAT_057 Values of EPS35

Property Name	**Value**
Density	35 kg/m^3
Young's Modulus	5.95 MPa
Hysteric Unloading	1
Shape	1
Tensile Stress Cutoff	0.1 MPa
Rate Sensitivity via damping coefficient	0.5
Nominal Stress vs Nominal Strain	Tabular Data

Table 4.3 MAT_063 Values of EPS35

Property Name	**Value**
Density	35 kg/m^3
Young's Modulus	5.95 MPa
Poisson's Ratio	0
Tensile Stress Cutoff	0.1 MPa
Rate Sensitivity via damping coefficient	0.5
Yield Stress vs Volumetric Strain	Tabular Data

Young's Modulus and Yield Stress vs Volumetric Strain datas were taken from performed uniaxial compression experiments. As mentioned in Section 3.3, $3500mm/min$ test data was chosen to use in analysis setup. Since Zwang et al. [25] presented that dependency of stress-strain curve of crushable foams to strain rate can be taken as negligible after a certain deformation speed. Also, Anlas and Ozturk [13] used 100mm/min compression speed data of specimen which had $50x50x50mm$ dimensions for impact analysis. They achieved pretty good results and proved this phenomenon again.

Since it is known that Poisson Ratio of crushable foam is equal to zero at non-linear elastic regime, Poisson Ratio of EPS35 was taken as 0. In addition, tensile stress cutoff and rate sensitivity via damping coefficient values of material card were initially taken from Shah and Topa study which includes drop test of EPS with 12.75kg/m^3 density [14].

After material assignments have been made, stiffness behavior of every part was determined and point mass was defined at the top of the impactor. This additional mass comes from parts which were not included into analysis setup such as accelerometer kit, clamps, pistol grip, ball arm etc.

Body Interactions were defined as frictional with 0.2 friction coefficient and meshing of foam has been made with sweep method and $5mm$ element size. Also, meshing of foam has been made with patch conforming method and $5mm$ element size to observe tetrahedron element effects. Foam which used as helmet's energy absorber liner might have more complex geometry and so, sweep method might not be suitable. Therefore, observing stiffener effect of tetrahedron elements and comparing them with experimental

results should be beneficial for future works of helmet design. Finite element analysis setup of 25 mm height foam are represented for both meshing method in Figure 4.6.

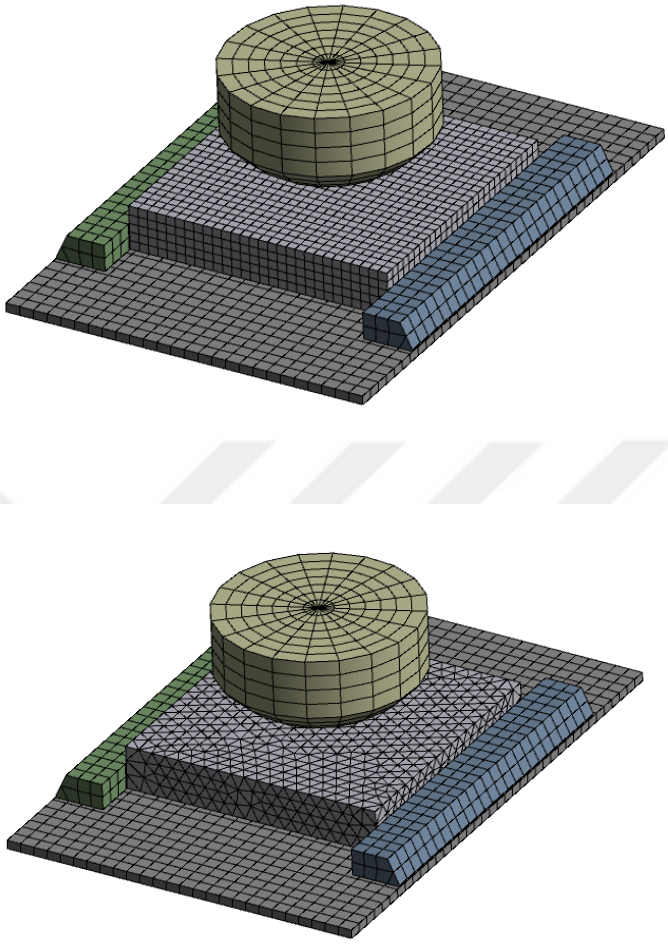

Figure 4.6 Meshing of analysis setup

Rigid body constrains were defined for all rigid parts and standard Earth gravity were added to achieve more realistic results. Additionally, hourglass control and different time step safety factor than default were assigned if needed. Finally, initial conditions determined according to MIL-DTL-87174A standard.

5. VERIFICATION OF FINITE ELEMENT MODEL

Since foams are used universally in a wide range of applications, a vast range of foams with significantly varied characteristics adapted individually to each end use has been developed according to their application areas. As described in previous sections, knowing every foams' behavior accurately is almost impossible. There are several generalized empirical equations to estimate their behavior. However, these equations cannot give accurate results especially on crushable foams. On the other hand, these equations depend on volume fraction of solid, volume fraction of edge to cell wall etc. and achieving this information from supplier for every case is not practicable. In addition, measuring volume fraction of edge to cell wall is very difficult operation and open to source of errors. Therefore, best way to learn compressive characteristics of single crushable foam is performing an experiment.

In this thesis, several experiments were conducted to observe stress strain curve of EPS35. However, it is known and shown that stress strain curve of EPS35 has strain rate dependency. Due to that reasons, several assumptions have been made according to studies in literature and initial finite element analysis model was created. This analysis model will be used in the later stage of design to decide structure of energy absorbing liner of flyers helmet. Since outer shell geometry of helmet is not known yet, simplified geometry was used in experiments to observe only foam characteristics.

Goal of these experiments is achieving acceleration versus time plots of impactor against crushable foam with different heights. After the observation of compressive behavior of EPS35 at MIL-DTL-87174A energy level and impactor shape, initial finite element model results were compared with experimental data. Then, modifications were conducted in finite element model if needed. At the end of the study, reaching finite element model which gives acceleration versus time result of impact within 10% error band is aimed. Peak acceleration value was not chosen as only aim of this study, because durations are also important according to energy absorption for helmet standards. Verified finite element model of EPS35 material would have key role on deciding final design of energy absorber liner because having safe and lightweight design is key parameter in helmets. Every single unnecessary mass means worthless force on flyer's neck and they can be cause of healthy critical situation.

5.1. Experimental Setup

To perform impact test on EPS35 samples, CADEX Monorail Impact Setup was used with embedded helmet test software. Also, some additional accessories which are mounting table and adjustment brackets were used to perform impact on EPS35 samples. CADEX Monorail Impact Setup was designed for performing headform impact test accurately and presented in Figure 5.1.

Figure 5.1 CADEX Monorail Impact Setup

In the test setup, all friction, height, velocity is controlled by initially given parameters and only output is acceleration data which is measured on center of impactor. In addition, impact velocity is measured by the help of the sensor located on the frame as seen in left side of Figure 5.2. Since design is made for headform test setup, stroke of impact is designed according to headform's height. However, foam samples had much less height than height form. For this reason, mounting plate was designed and produced to level up foam positions. Also, adjustment brackets were located on this mounting plate to guide foam specimens. By the help of these, foam samples were leveled up and centered according to impactor position. Final test setup is presented in the right side of Figure 5.2.

Impact velocity measurement

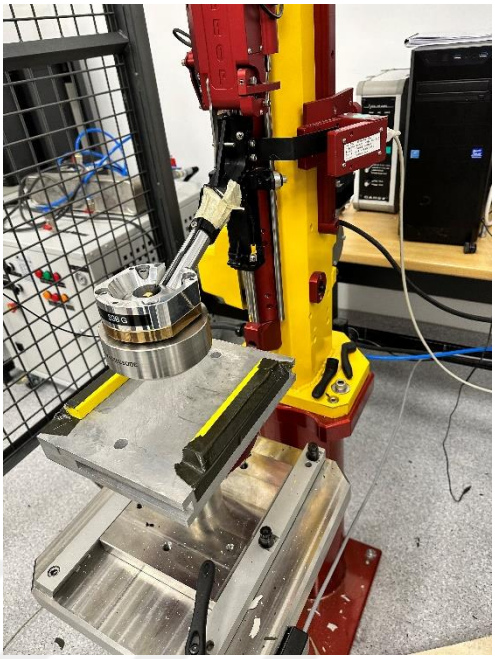

Modified test setup

Figure 5.2 Experimental Setup

In test procedure, following configuration was applied and configuration management has been made on embedded software.

Table 5.1 Instruments of Impact Setup

Description	**Mass**
Spherical Impactor	3068g
Split Ring Clamp	536g
Pistol Grip	684g
4 Bolts for Clamp	82g
Accelerometer Kits	10g
Ball Arm Aluminum	620g
Total	**5000g**

8 tests were performed on CADEX Monorail Impact setup. In these tests, foam specimens which are presented in Figure 5.3 were used. These specimens had $40, 35, 30$ and $25mm$ heights tests and they were conducted with $35\ foot-pounds$ $(47.45\ J)$ energy for applied impact. Experiments were re-applied for every thickness value of foam specimen

to observe repeatability of test and minimize test error. Also, all of the experiments were recorded in 240 fps since impact speed was too high to observe every steps of impact clearly. As an example, several sections of impact test of 35mm height specimen are given in Figure 5.4.

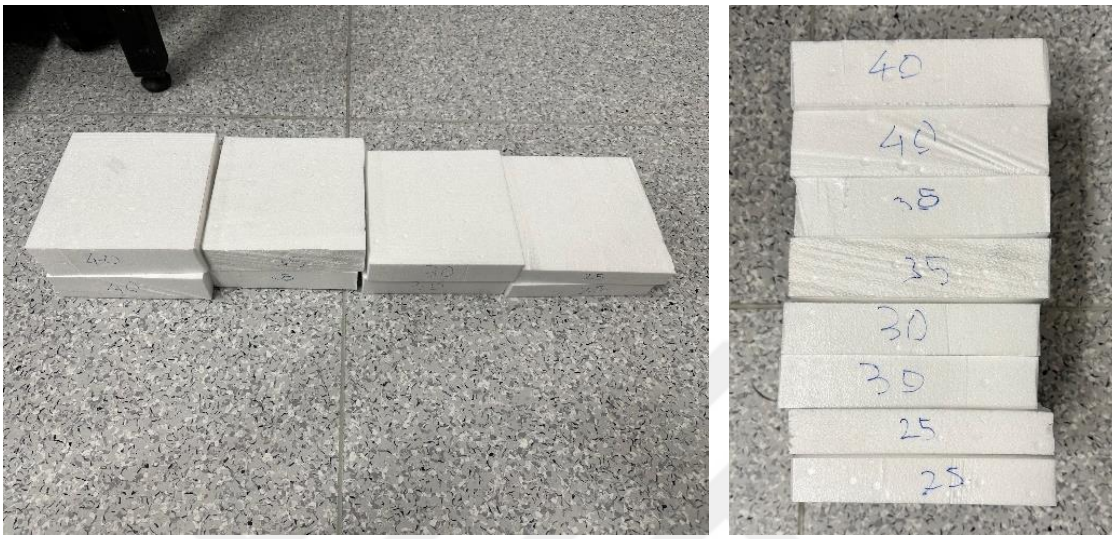

Figure 5.3 Foam Specimens

To apply $47.45J$ impact energy, impact velocity of impactor which has $5\ kg$ mass was chosen as $4.36\ m/s$. As mentioned above, impact velocity is also measured by sensor and it was seen that impact velocity of every experiment were occurred in 2% error band.

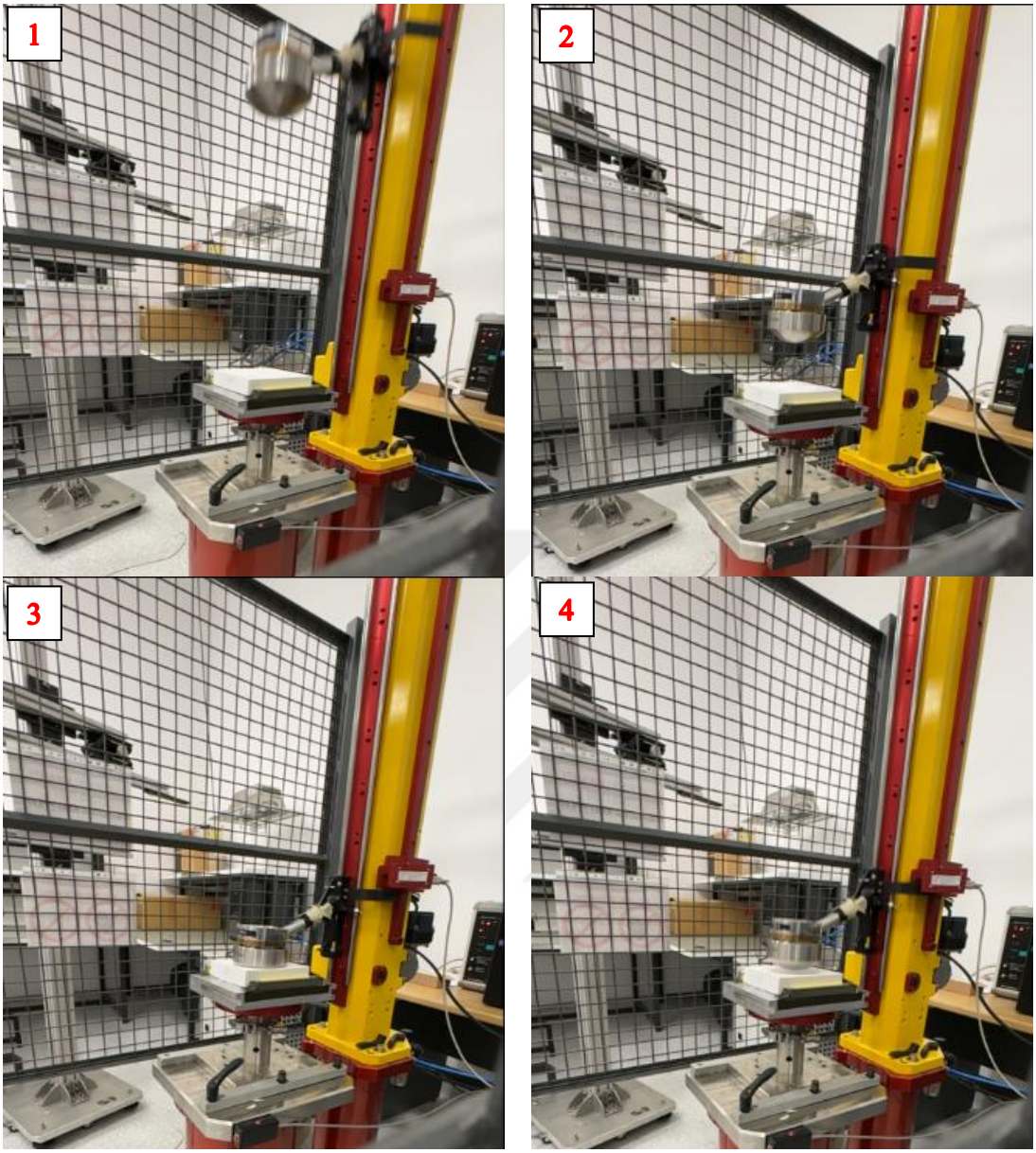

Figure 5.4 Impact test of 35mm height specimen

5.2. Results & Comparison

5.2.1. Experimental Results

Results of impact experiments are presented in this section of thesis. Also, impact velocities and peak g values are given in Table 5.2. In results, it is observed that all acceleration data were matched to corresponding second experiment data.

Table 5.2 Experimental Results

Number of Impact	Foam Thickness	Impact Velocity (m/s)	Peak g Value
1	40±0.5mm	4.4068	88.5
2	40±0.5mm	4.3804	86.2
3	35±0.5mm	4.3870	88.1
4	35±0.5mm	4.3942	88.5
5	30±0.5mm	4.3783	95.6
6	30±0.5mm	4.4525	95.6
7	25±0.5mm	4.3959	112.5
8	25±0.5mm	4.3564	112.1

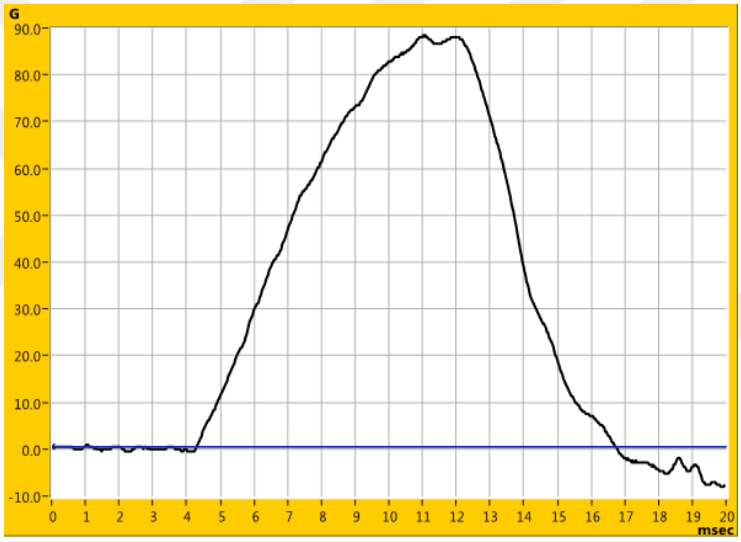

Acceleration[g] vs Time[ms] Graph of #1 Impact

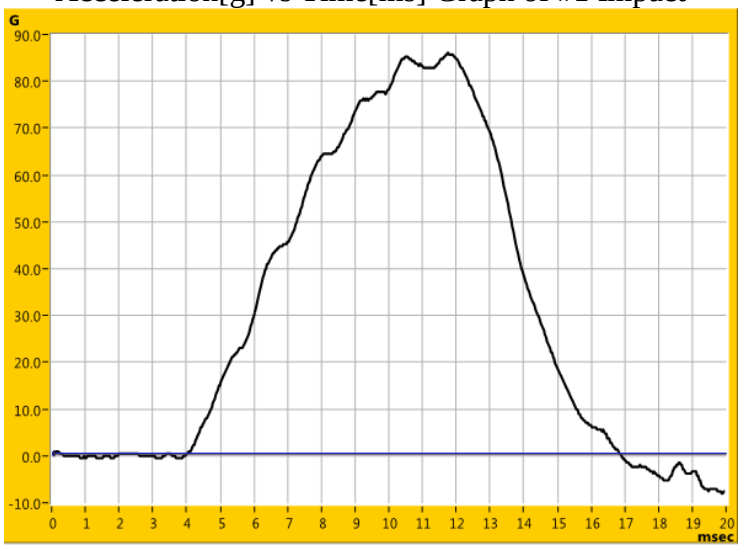

Acceleration[g] vs Time[ms] Graph of #2 Impact

Figure 5.5 Experimental Results of Specimens Which Have 40mm Height

Experimental results of specimens which have 40mm height are presented in Figure 5.5. Although acceleration of #2 impact is more scattered, peak acceleration values and impact duration were matched.

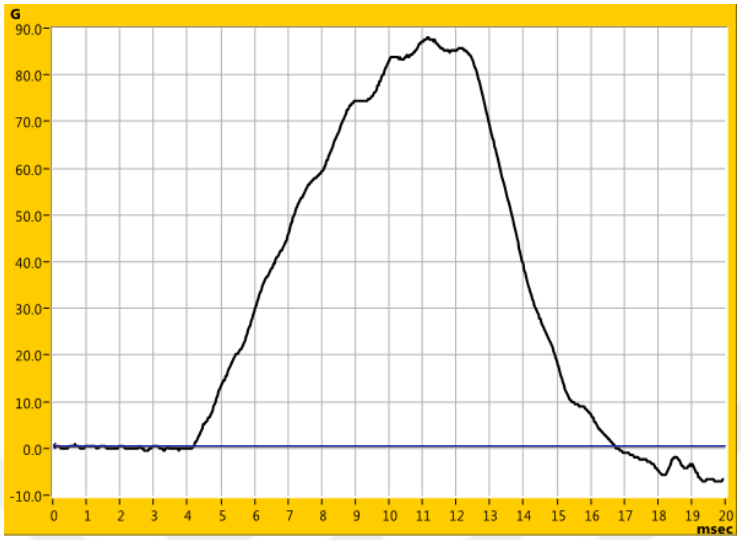

Acceleration[g] vs Time[ms] Graph of #3 Impact

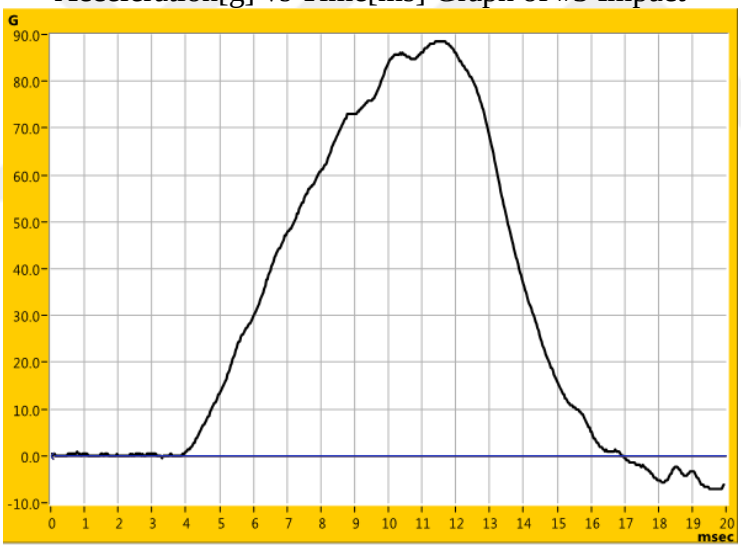

Acceleration[g] vs Time[ms] Graph of #4 Impact

Figure 5.6 Experimental Results of Specimens Which Have 35mm Height

Experimental results of specimens which have 35mm height are presented in Figure 5.6. Peak acceleration values and impact duration of both experiments were almost same.

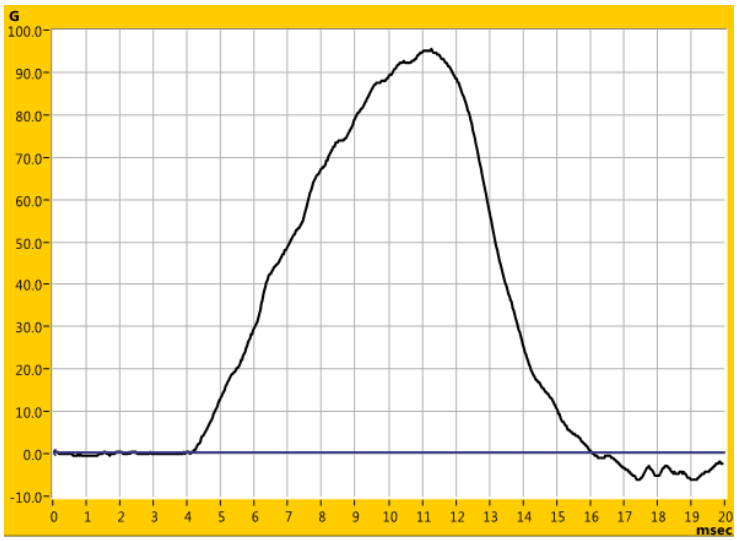

Acceleration[g] vs Time[ms] Graph of #5 Impact

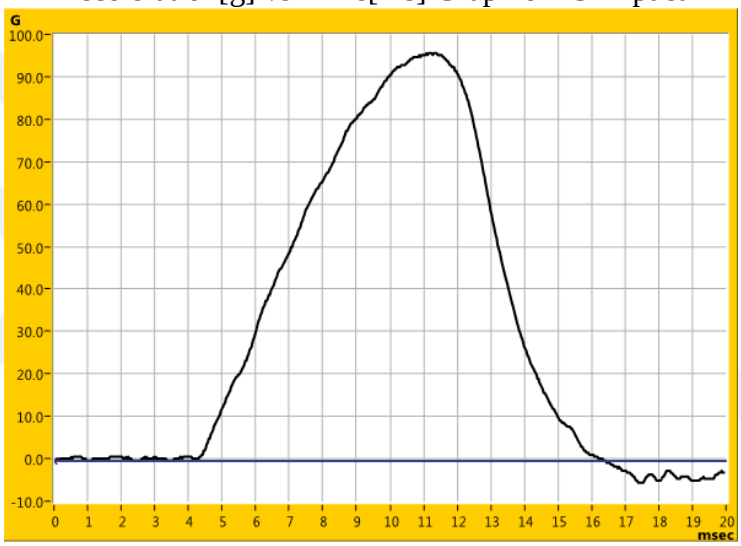

Acceleration[g] vs Time[ms] Graph of #6 Impact

Figure 5.7 Experimental Results of Specimens Which Have 30mm Height

Experimental results of specimens which have 30mm height are presented in Figure 5.7. Although acceleration of #5 impact is more scattered, peak acceleration values and duration of both impacts were perfectly matched.

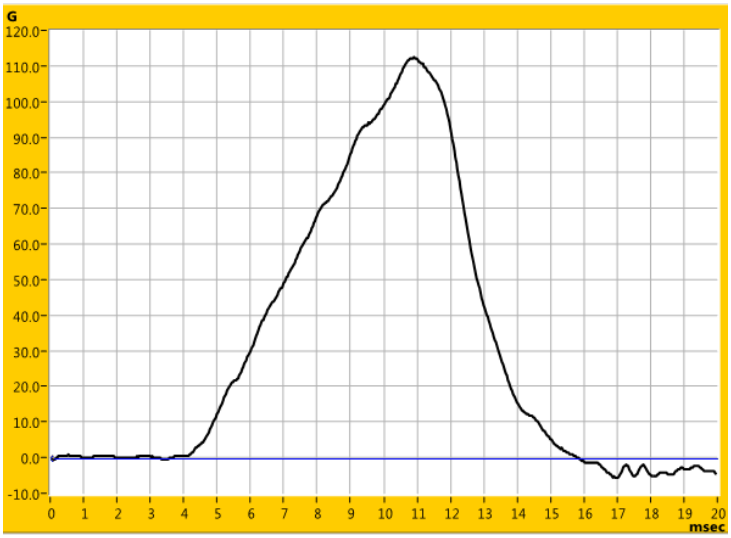

Acceleration[g] vs Time[ms] Graph of #8 Impact

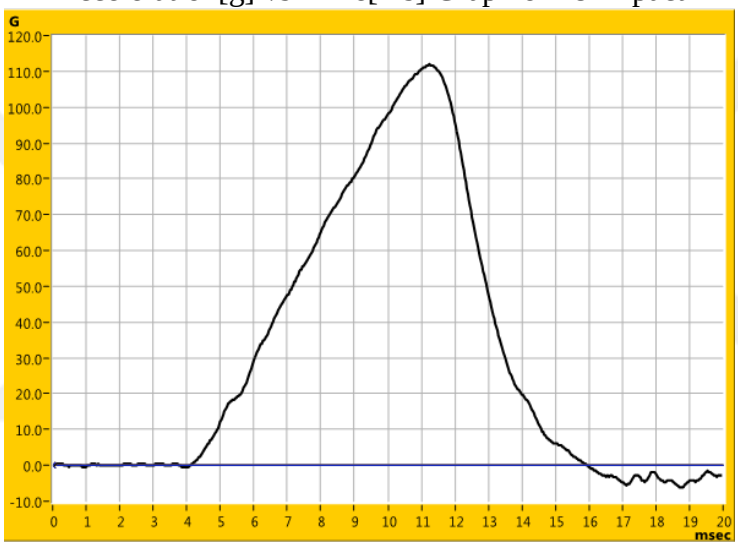

Acceleration[g] vs Time[ms] Graph of #8 Impact

Figure 5.8 Experimental Results of Specimens Which Have 25mm Height

Experimental results of specimens which have 25mm height are presented in Figure 5.8.

Peak acceleration values and impact duration of both experiments were almost same.

As can be seen from the results, the acceleration reaches zero in a shorter time after reaching its peak value. For this reason, it is important to get the entire acceleration graph accurately. A faster decrease in acceleration will result in less time spent at high g values and compliance with the standard will become easier.

5.2.2. Finite Element Model Development

As mentioned in Section 4.3, hourglass energy was monitorized simultaneously during the finite element analysis to check hourglass energy and law of energy conversation. There were little hourglass energy development for hexahedral solid element although Belytschko-Bindeman Lienar Total Strain hourglass control was used. In default, LS-DYNA creates constant stress solid element (LS-Dyna ID: 1) which has reduced integration formulation. Although the developed hourglass energy was relatively small to total energy, solid element formulation was changed to fully integrated S/R solid element with efficient formulation (LS-Dyna ID: -2). On the other hand, tetrahedral mesh version of analysis setup was used by default element formulation which is 1 point tetrahedron (LS-Dyna ID: 10). By using 4 node linear 1 point integration mesh, no hourglass energy was observed, since hourglass can occur only in 8 node hex solids and 4 node quad shells. This linear 4 node tetrahedron element was known as too stiff so that it is not recommended. However, it is the most time efficient tetrahedron element formulation and this recommendation is not valid for foams [30]. Therefore, 1 point tetrahedron was chosen as element formulation of tetrahedron mesh by considering that time step of tetrahedral is mesh much lower than time step of hexahedral mesh which has same element size. Additionally, observing accuracy of most simple tetrahedral mesh would be beneficial at end stages of design, since analysis model could be much larger and time efficiency of mesh would be another important parameter. As an example, model development according to hourglass energy of 25mm height foam is given in Figure 5.9.

To get accurate finite element model, material cards of foam also modified. In modelling of EPS35, MAT57 and MAT63 are used as mentioned before. In these material cards, there are several parameters to determine in addition to the load curve of foam, Young's Modulus and Poisson Ratio. These parameters are tensile cutoff stress, hysteretic unloading, shape factor and damping for MAT57, tensile cutoff stress and damping for MAT63.

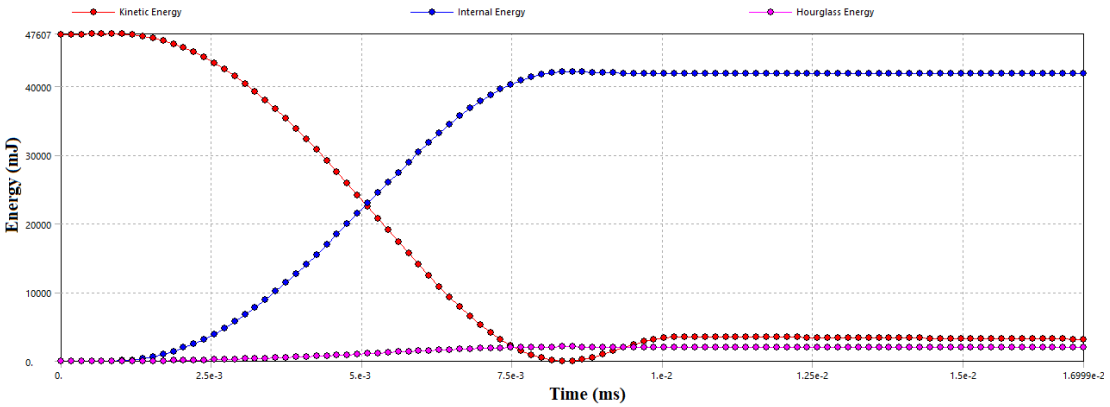

Default Hexahedral Element Without Hourglass Control

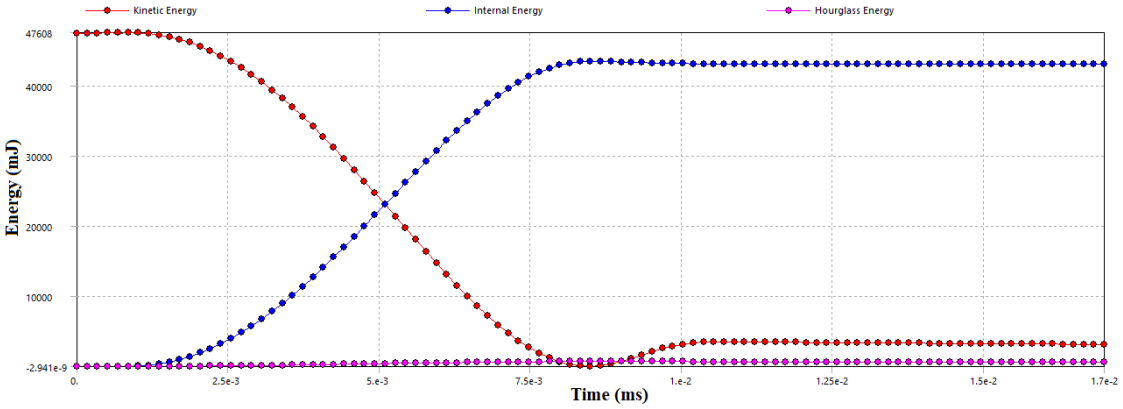

Default Hexahedral Element With Hourglass Control

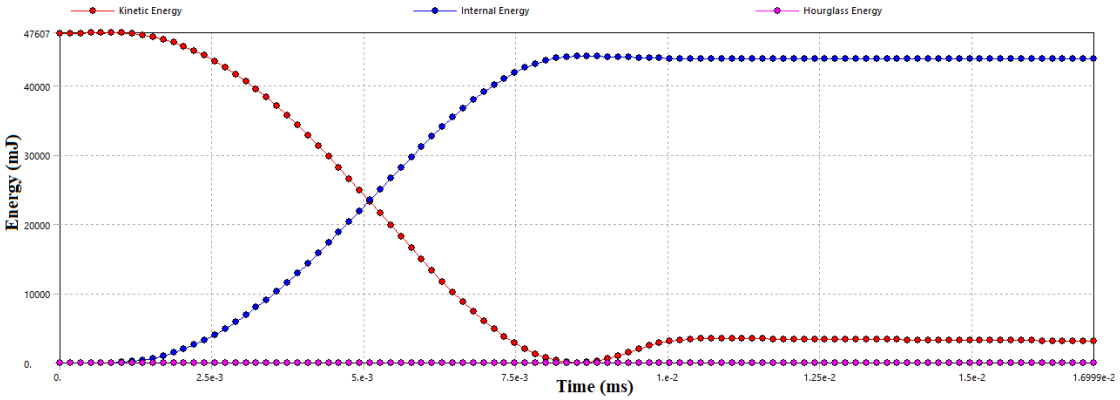

Fully Integrated Hexahedral Element Without Hourglass Control

Figure 5.9 Model Development According to Hourglass Energy of 25mm Height Foam

Tensile cutoff stress represents cut-off for the nominal tensile stress and damping value presents viscous coefficient of model and recommended value is in between 0.05 and 0.5 for realistic setup. Tensile cutoff stress and damping coeffcient were found from literature for EPS [14]. Therefore, MAT63 material card cannot be modified by these parameters. On the other hand, it can be manipulated by loading curve datas, since elasticity of unloading curve of MAT63 depends on final slope of load curve. By changing last values of compressive load curve datas, unloading curve of foam can be changed. However, this change would be limited and unrealistic and will be source of error at high strains.

In MAT57 material card, the hysteretic unloading value has to be in between 0 and 1. In default, this is equal to 1 and it represents no energy dissipation. Hysterisis is getting larger while hysteric unloading factor value closes to 0. Value of hysteretic unloading factor also affects shape factor. Shape factor is activated when hysteretic unloading factor has nonzero value. Shape factor value increases energy dissipation when it is greater than one and vice versa. Value of these parameters were determined by trial-and-error method. All developed final finite element models parameters are presented in Table 3.1.

Table 5.3 Final Finite Element Models Parameters

Parameters	**#1 FE Model**	**#2 FE Model**	**#3 FE Model**	**#4 FE Model**
Element LS-Dyna ID	-1	10	-1	10
Element Size	5mm	5mm	5mm	5mm
Material Card	MAT_057	MAT_057	MAT_063	MAT_063
Damping Coefficient	0.5	0.5	0.5	0.5
Tensile Stress Cut-off	0.1MPa	0.1MPa	0.1MPa	0.1MPa
Hysteretic Unloading	0.001	0.001	NA	NA
Shape	10	10	NA	NA
Poisson Ratio	NA	NA	0	0
Load Curve	Data of 3500mm/min test	Data of 3500mm/min test	Data of 3500mm/min test	Data of 3500mm/min test
Young's Modulus	5.95 MPa	5.95 MPa	5.95 MPa	5.95 MPa
Density	35 kg/m^3	35 kg/m^3	35 kg/m^3	35 kg/m^3

5.2.3. Results Comparison

In this stage of thesis, four different finite element analysis were compared with experimental results in a single plot for every experiment. Error band according to experimental results was determined as ±0.5 milliseconds and ±5% of peak g value.

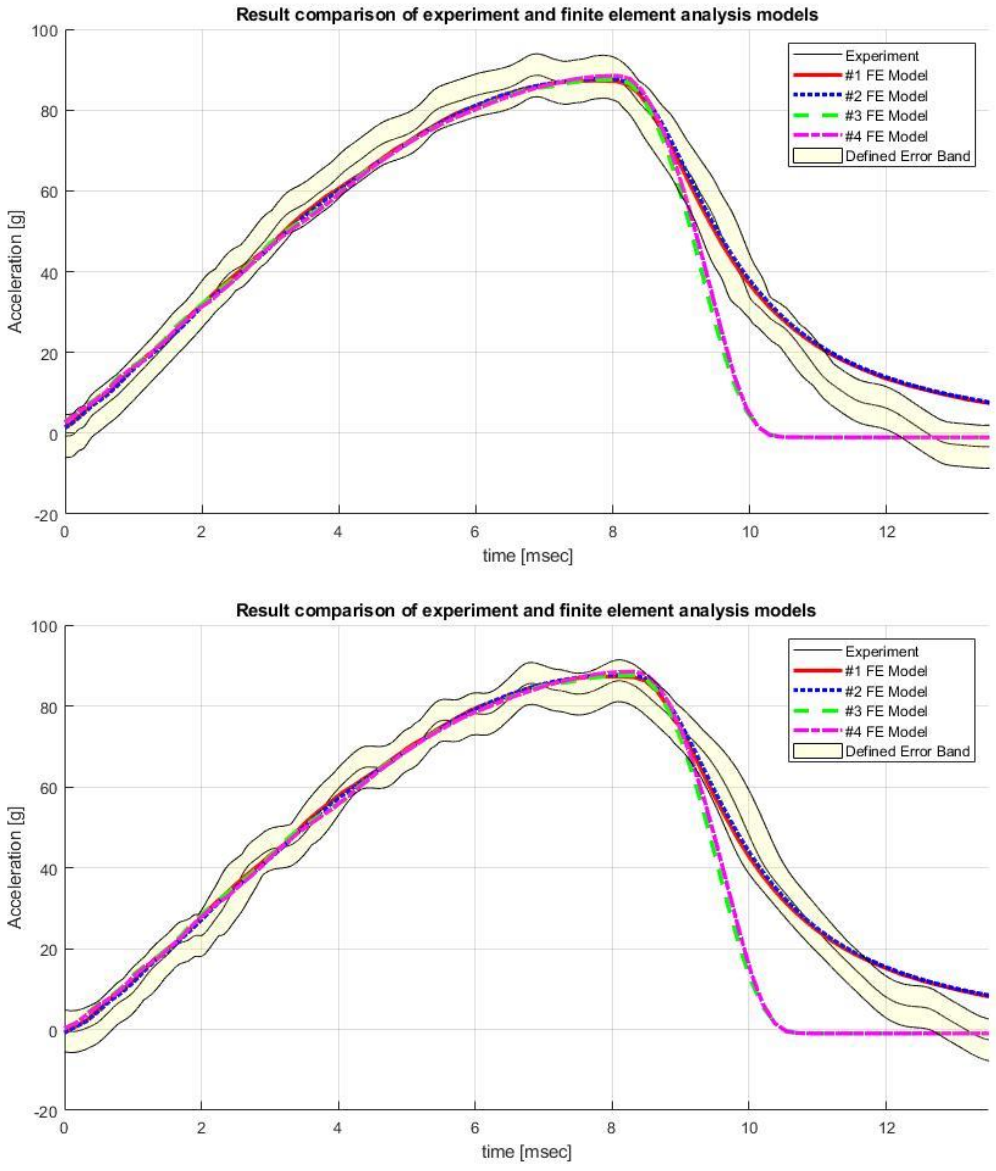

Figure 5.10 Result Comparison of Specimens Which Have 40mm Height

FE analysis and experimental results of specimens which have 40mm height are presented in Figure 5.10. It is seen that there is no significant difference between hexahedral and tetrahedron element. On the other hand, the difference was observed between MAT_063 and MAT_057 material card. FE analysis can simulate impact successfully by using both

material cards until the peak acceleration. However, unloading behavior of MAT_063 material card is fully elastic and limited. Therefore, MAT_063 material card cannot simulate correctly the dynamics of impact after the peak acceleration reached while MAT_057 material card simulates successfully.

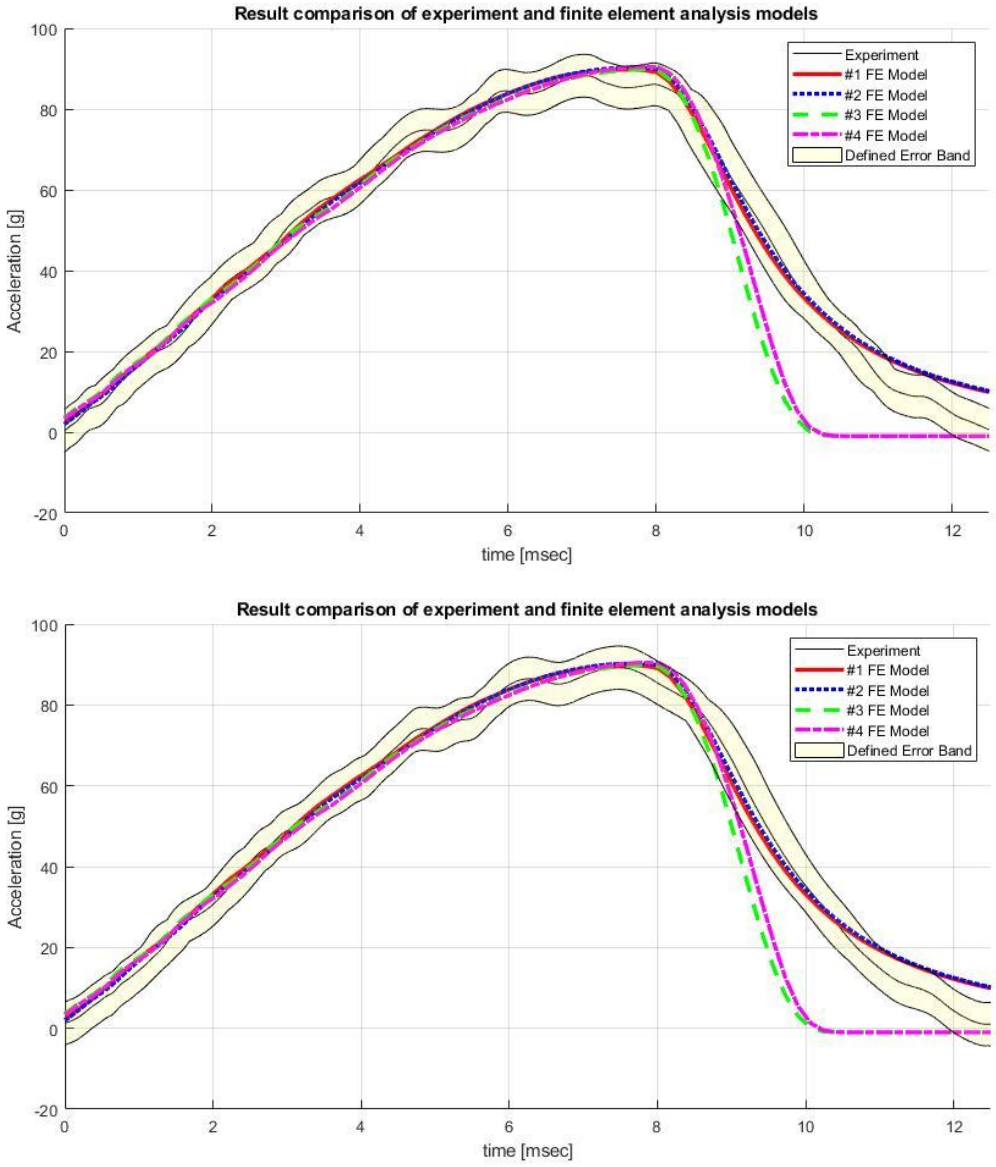

Figure 5.11 Result Comparison of Specimens Which Have 35mm Height

FE analysis and experimental results of specimens which have 35mm height are presented in Figure 5.11. It is seen that there is no significant difference between hexahedral and tetrahedron element. On the other hand, the difference was observed between MAT_063 and MAT_057 material card. FE analysis can simulate impact successfully by using both material cards until the peak acceleration. However, unloading behavior of MAT_063

material card is fully elastic and limited. Therefore, MAT_063 material card cannot simulate correctly the dynamics of impact after the peak acceleration reached while MAT_057 material card simulates successfully.

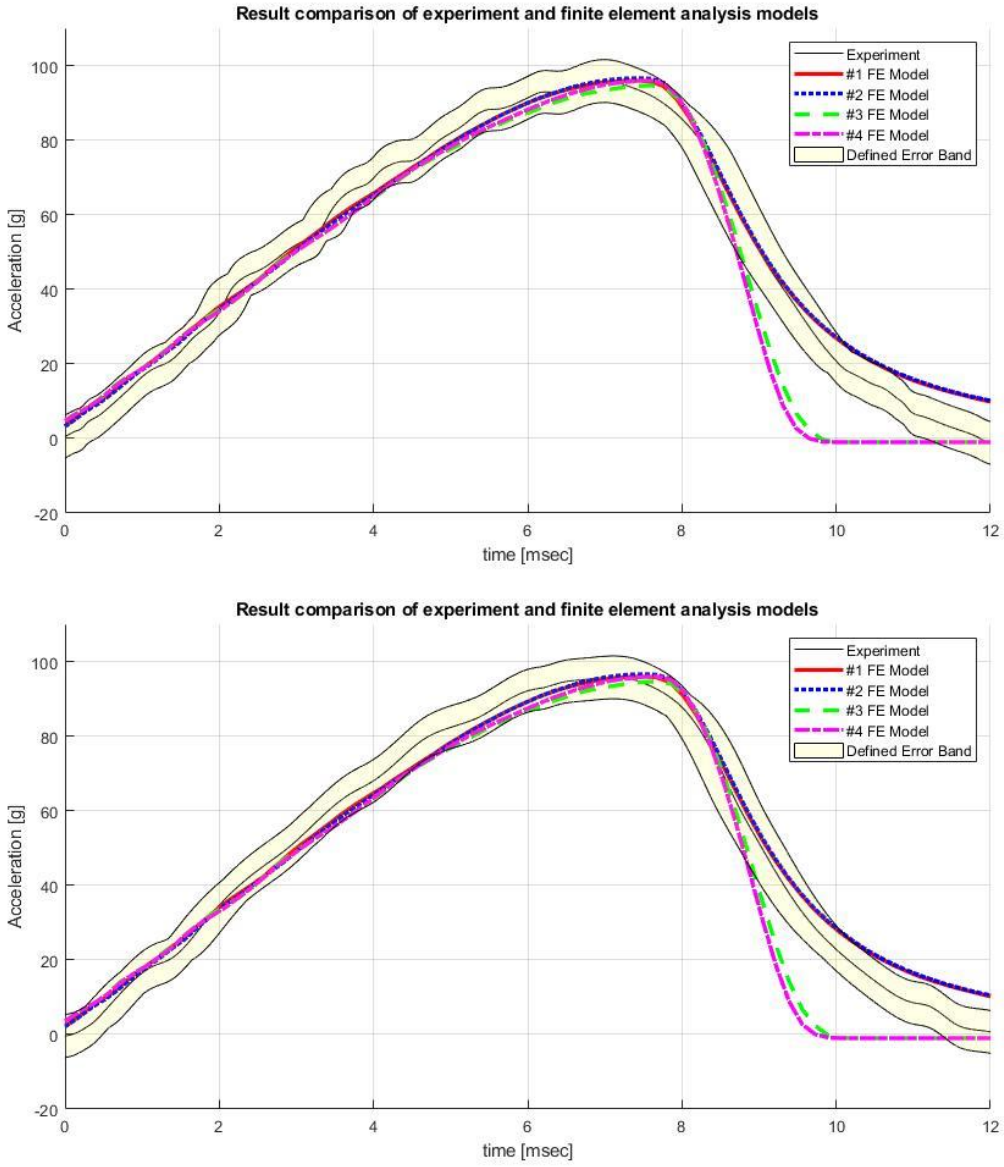

Figure 5.12 Result Comparison of Specimens Which Have 30mm Height

FE analysis and experimental results of specimens which have 30mm height are presented in Figure 5.10. It is seen that there is no significant difference between hexahedral and tetrahedron element. On the other hand, the difference was observed between MAT_063 and MAT_057 material card. FE analysis can simulate impact successfully by using both material cards until the peak acceleration. However, unloading behavior of MAT_063

material card is fully elastic and limited. Therefore, MAT_063 material card cannot simulate correctly the dynamics of impact after the peak acceleration reached while MAT_057 material card simulates successfully.

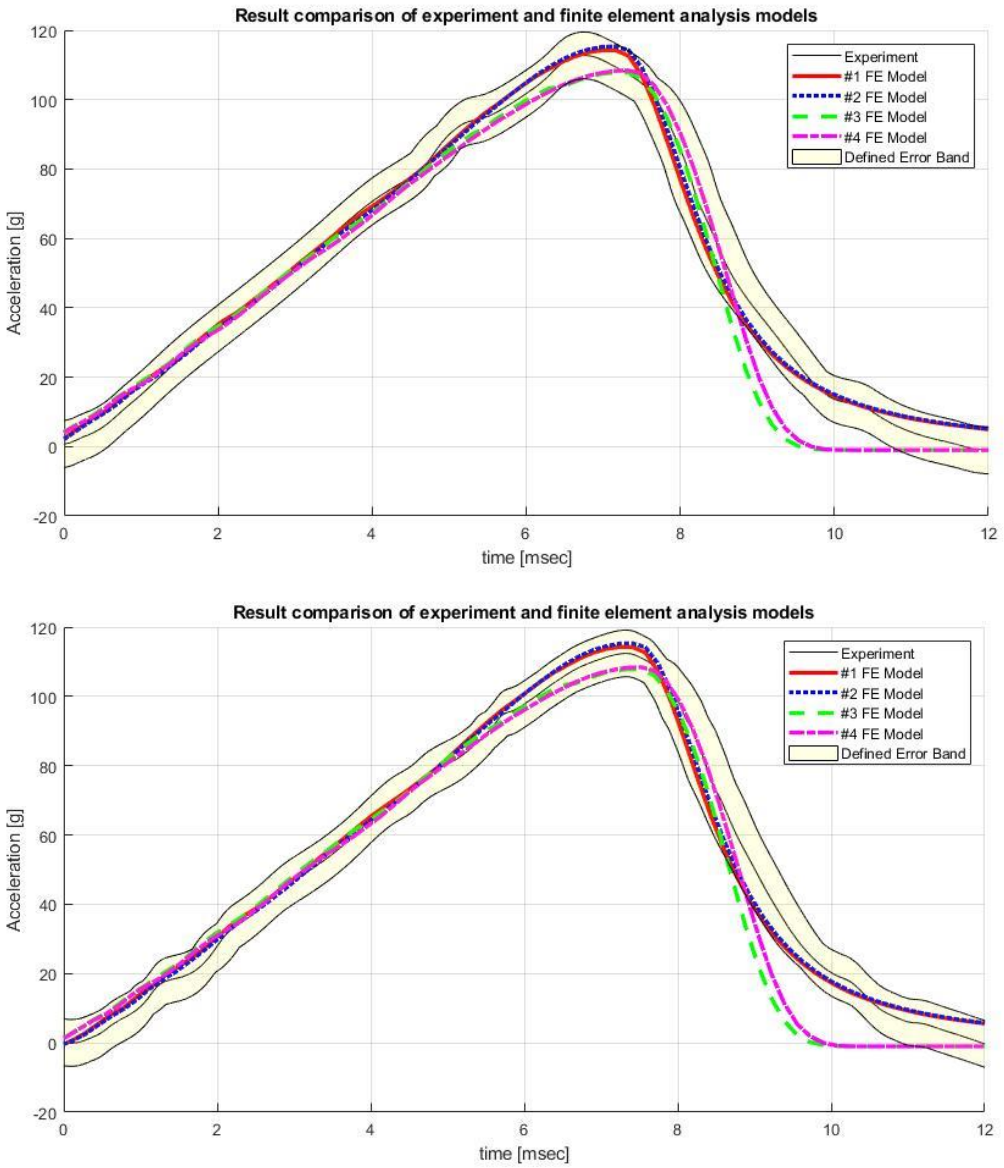

Figure 5.13 Result Comparison of Specimens Which Have 25mm Height

FE analysis and experimental results of specimens which have 25mm height are presented in Figure 5.13. It is seen that there is no significant difference between hexahedral and tetrahedron element. On the other hand, the difference was observed between MAT_063 and MAT_057 material card. MAT_063 material card cannot simulate correctly the dynamics of impact for last 3ms while MAT_057 material card simulates the whole impact successfully.

6. RESULTS AND CONCLUSION

The impact shocks are crucial for flyers and helmets. Due to high kinetic energy and low impact durations it can cause neck injury and brain damage or even death. In the design stage, the helmet exposed to these impacts must be carefully analyzed. In this thesis, impact analysis of energy absorption liner material of flyer's helmet is investigated.

The purpose of this study is obtaining accurate finite element analysis model of crushable foam which is used in the design stage of helmet. Generally, maximum acceleration in the headform is used as head injury criterion. Acceptable maximum acceleration varies depending on application, since head injury is time dependent to resultant acceleration as stated at Wayne State Tolerance Curve (WSTC). There are several standards which are based on WSTC which determines time and acceleration boundaries of impact results. In this thesis, MIL-DTL-87147A is a predefined requirement document which covers the HGU-55/P flyer's helmet requirements.

When the foams are investigated, it is observed that there are enormously variety of foams on the market due to their wide application areas. Their material, morphology or density are changing in almost every product. In brief, foams are divided into two which are closed cell and open cell foams based on their morphology. Also, both open cell and closed cell foams are divided into 3 according to their matrix material behavior. They can be listed such as foams that undergoes elastic collapse, plastic collapse and brittle crushing. On the other hand, their density can vary depending on volume fraction of matrix material to foam. In the requirements of MIL-DTL-87174A material of energy absorption liner is limited. In this military specification document, material of liner is determined as EPS having a density of 2 – 2.5 pounds per cubic foot (32.04 – 40.05 kilograms per cubic meter). EPS has rigid polymer matrix material and closed cell morphology. Also, it is one of the most efficient energy absorption material in rigid polymers, since weight is crucial parameter in helmet design. Energy absorption capabilities per weight has the first priority in material selection. To have enough absorption specification and low weight, density of EPS was limited in requirements document. Therefore, density of EPS was chosen as 35 kg/m^3 in this study.

There are several empirical formulations in literature to determine compressive behavior of foams. However, empirical results vary widely with respect to best line of overall results especially in closed cell foams. Also, general behavior of closed cell foams has been determined in terms of volume fraction of cell wall against edge, relative density, volume fraction of solid. As can be estimated, achieving or measuring these parameters in this variety of foams is very difficult and open to source of errors.

A validated and accurate finite element model has a key role in the design stage, because the thickness, shape and weight of the energy absorber liner directly depends on analysis results. Making an experiment in every stage of design is not cost and time effective especially for product which require molding in production stage such as helmet. Therefore, obtaining accurate results from finite element analysis has a critical role. Creating accurate FE model of EPS is not possible due to complexity of material and uncertainties. Also, compressive behavior of EPS can vary with strain rate. For these reasons, several experiments and analyses have been conducted to achieve validated material model in desired strain rate and energy level.

One of the encountered problems in creating material model was to get stress-strain data of EPS at defined impact velocity. To observe meaningful stress-strain data, several uniaxial compression experiments have been conducted at different strain rates. Compression velocities of experiments were $2mm/min$, $3000mm/min$ and $3500mm/min$. In these experiments, strain rate dependency of EPS35 was observed with no doubt. As seen, maximum compression velocity was $3500mm/min$ in these experiments, since it was maximum allowable compression speed supplied by DARTEC uniaxial compression machine. It is known from the literature that dynamic behavior of EPS does not change significantly after certain compression velocity. Therefore, stress-strain data of experiment which obtained with $3500mm/min$ compression speed was taken as load curve of material model.

Other problems faced in finite element building process were negative volume error and hourglass energy development. Negative volume error is seen when a material undergoes extremely large deformations. Under these deformations, an element might become so distorted and this causes volume of the element may be calculated as negative even element does not reach to failure criteria. It is generally observed in foam analysis under

impact. There are several methods to overcome these negative volume error problems. Firstly, material can be modelled as stiffer at large strains. Also, tailoring the initial mesh of distorted elements is recommended to overcome this problem. Reducing time scale factor can be another option to prevent numerical instabilities. In this study, changing stress-strain curve of material was not chosen. Moreover, negative volume problem was seen in almost all elements. Therefore, tailoring the mesh of distorted elements was not a solution. To overcome this problem, failure criteria which is defined as tensile stress cutoff in these material models was investigated. The gathered tensile stress cutoff value from the literature and reducing time scale factor for hexahedral elements to "0.6" from default value "0.9" solved the problem. For law of conversation of energy violations, firstly hourglass control methods used although developed hourglass energy was not exceeds 10% of system energy. After the application of Belytschko-Bindeman Lienar Total hourglass control, generated non-physical hourglass energy dropped significantly. However, it was still exist. To have zero hourglass, fully integrated element formulations was chosen for hexahedral elements. By that way, all of hourglass energy was cancelled.

To create accurate finite element model of foam under impact, LS-Dyna was chosen as explicit solver. Material cards of LS-Dyna and accurate finite element models of crushable foams in the literature have been investigated. There are lots of foam material cards in LS-Dyna due to variety of foams. It is seen from the literature that MAT57 and MAT63 are most appropriate material cards which are defined in LS-Dyna library. MAT57 is used for low density foam which has full recovery such as seat cushions. On the other hand, MAT63 material card is designed for crushable foam with limited elastic recovery. However, during uniaxial compression tests, it is observed that EPS has remarkable recovery at high strain rates although it is considered as brittle crushing foam and has limited recovery. Therefore, both material cards cannot represent dynamic behavior of EPS initially. Although they can simulate loading behavior of EPS under impact, both of them did not represent correct unloading path of crushable foam at the beginning. To overcome this problem, equations of these material cards were examined. Then, it was seen that modification of unloading behavior of MAT63 is not possible without manipulate the stress-strain data of model. In this card, unloading behavior of foam is elastic to last slope of loading curve. Changing slope of unloading curve is possible only by entering unrealistic stress-strain data to the model. On the other hand, there are several parameters to tune unloading curve of MAT57 material card which are

named as hysteric unloading and shape factor. In finite element development process, values of these parameters have been found by trial-and-error method.

At the end of finite element development process, four different finite element model results were compared with experimental data. This comparison was applied for 8 different experiment with 4 different heights of foam. At the same time, an error band was defined for comparison. In definition of error band, parameters selected as ±0.5 milliseconds and ±5% of peak g value through all acceleration versus time curve of experiments. According to results, it is obtained that there is no considerable difference between foams modeled with hexahedral or tetrahedral element. Both element formulations can be used in further stages with these material cards. Also, it is seen that MAT57 is better choice to simulate crushable foam behavior under impact loadings. It gives accurate results along the acceleration curve excepts comparably small section at the end for some cases. As mentioned in previous stages, resultant acceleration is not the only parameter to prevent head injuries. Time is also important parameter and MAT57 material card gives more accurate results through the curve. Although MAT63 material card simulates acceleration response until the peak acceleration successfully, it shows quick recovery motion. For this reason, MAT63 does not follow experimental results while acceleration decreases. However, simulating acceleration correctly just before and after the peak has the most valuable point in impact analysis of helmet because MIL-DTL-87174A limits the peak acceleration by 400g and also, the recorded acceleration shall not exceed 150g for more than 6 milliseconds and 200g for 3 milliseconds. Therefore, observed errors in some cases of finite element model which uses MAT57 material model can be taken as negligible because the section where the error occurs is far away from the peak values.

To sum up, the results obtained from finite element model by using MAT57 material card and experiments are quite satisfactory for all cases and it will shed light on design determination studies in the following stages.

REFERENCES

[1] B. Croop, H. Lobo, N. DatapointLabs, Selecting material models for the simulation of foams in LS-DYNA, 7th European LS-Dyna conference, 2009, pp. 1-6.

[2] D. Al-Tinawi, Foam modelling and application to Sabot impact, (2007).

[3] A. Droste, J. Rögger, Crash performance increase with structural BETAFOAMTM, Proceedings of the LS-DYNA Anwenderforum, (2007) 37-44.

[4] J.D. Reid, R.W. Bielenberg, Modeling rebound of foam backed racetrack barriers, Proceedings of the 10th International LS-DYNA® Users Conference, 2008, pp. 43-50.

[5] R.W. Bielenberg, J.D. Reid, Modeling crushable foam for the SAFER racetrack barrier, 8th International LS-DYNA Users Conference, 2004, pp. 1-10.

[6] P.K. Pinnoji, P. Mahajan, N. Bourdet, C. Deck, R.m. Willinger, Impact dynamics of metal foam shells for motorcycle helmets: Experiments & numerical modeling, International Journal of Impact Engineering, 37 (2010) 274-284.

[7] M. Barsotti, Comparison of FEM and SPH for Modeling a Crushable Foam Aircraft Arrestor Bed, 11th International LS-DYNA Users Conference, (2010).

[8] CRP Subsea, Crushable Foam Wrap, https://www.crpsubsea.com/products/product-families/downhole-protection/crushable-foam-wrap/.

[9] G. Downie, Crushable foam wrap mitigates subsea casing failures, Hart's E & P, 82 (2009) 67-69.

[10] B. Sambamoorthy, T. Halder, Characterization and component level correlation of energy absorbing (EA) polyurethane foams (PU) using LS-DYNA material models, Proceedings of the third LS_DYNA European conference, 2001.

[11] Q. Liu, G. Subhash, X.-L. Gao, A parametric study on crushability of open-cell structural polymeric foams, Journal of Porous Materials, 12 (2005) 233-248.

[12] G. Slik, G. Vogel, V. Chawda, D. Automotive, Material model validation of a high efficient energy absorbing foam, Proceedings of the 5th LS-DYNA Forum, Citeseer, 2006.

[13] U.E. Ozturk, G. Anlas, Finite element analysis of expanded polystyrene foam under multiple compressive loading and unloading, Materials & Design, 32 (2011) 773-780.

[14] Q.H. Shah, A. Topa, Modeling Large Deformation and Failure of Expanded Polystyrene Crushable Foam Using LS-DYNA, (2014).

[15] U. ÇALIŞKAN, M. APALAK, FEM ANALYSES OF LOW VELOCITY IMPACT BEHAVIOUR OF SANDWICH PANELS WITH EPS FOAM CORE, JOURNAL OF THERMAL ENGINEERING, 3 (2017).
[16] W. Chen, H. Hao, D. Hughes, Y. Shi, J. Cui, Z.-X. Li, Static and dynamic mechanical properties of expanded polystyrene, Materials & Design, 69 (2015) 170-180.
[17] G. Machado, M. Alves, R. Rossi, C. Silva Jr, Numerical modeling of large strain behavior of polymeric crushable foams, Applied Mathematical Modelling, 35 (2011) 1271-1281.
[18] B. Zhang, X. Zhang, S. Wu, H. Zhang, Indentation of expanded polystyrene foams with a ball, International Journal of Mechanical Sciences, 161 (2019) 105030.
[19] O. Ramon, J. Miltz, Prediction of dynamic properties of plastic foams from constant–strain rate measurements, Journal of applied polymer science, 40 (1990) 1683-1692.
[20] M.F. Ashby, L.J. Gibson, Cellular solids: structure and properties, Press Syndicate of the University of Cambridge, Cambridge, UK, (1997).
[21] R.M. Sullivan, L.J. Ghosn, B.A. Lerch, A general tetrakaidecahedron model for open-celled foams, International Journal of Solids and Structures, 45 (2008) 1754-1765.
[22] H.L.A. Van Den Bosch, Crash helmet testing and design specifications, (2006).
[23] E.S. Gurdjian, V. Roberts, L.M. Thomas, Tolerance curves of acceleration and intracranial pressure and protective index in experimental head injury, Journal of Trauma and Acute Care Surgery, 6 (1966).
[24] Military Specifications and Standards, MIL-DTL-87174A - DETAIL SPECIFICATION: HELMET, FLYER'S HGU-55/P, 1998.
[25] J. Zhang, N. Kikuchi, V. Li, A. Yee, G. Nusholtz, Constitutive modeling of polymeric foam material subjected to dynamic crash loading, International journal of impact engineering, 21 (1998) 369-386.
[26] Livermore Software Technology (LST), LS-DYNA User's Manual, Vol. II– Material Models, 2021.
[27] ANSYS Inc., Advanced Analysis Techniques Guide.
[28] Livermore Software Technology (LST), LS-DYNA User's Manual, Vol. I, 2021.
[29] M.T. Islam, E.A. Singh, Study of behavior of RCC beam under impact loading and effect of hourglass energy by finite element analysis using ANSYS, IJERT, 8 (2019) 2278-0181.

[30] ANSYS Inc., Ansys Workbench LS-DYNA, Element Formulations, 2021.